JACS
JOURNAL OF THE AMERICAN CHEMICAL SOCIETY
Article
pubs.acs.org/JACS

Photophysical and Computational Investigations of Bis(phosphine) Organoplatinum(II) Metallacycles

J. Bryant Pollock, Timothy R. Cook, and Peter J. Stang*

Department of Chemistry, University of Utah, 315 South 1400 East, Salt Lake City, Utah 84112, United States

Supporting Information

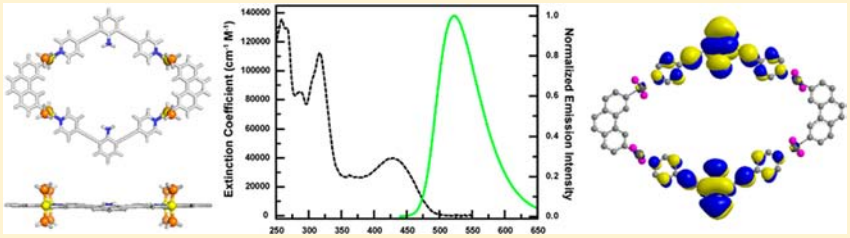

ABSTRACT: A series of endohedral and exohedral amine-functionalized ligands were synthesized and used in the construction of supramolecular D_{2h} rhomboids and a D_{6h} hexagon. These supramolecular polygons were obtained via self-assembly of 120° dipyridyl donors with 180° or 120° diplatinum precursors when combined in 1:1 ratios. Steady-state absorption and emission spectra were collected for each ligand and metallacycle. Density functional theory (DFT) and time-dependent DFT calculations were employed to probe the nature of the observed optical transitions for the rhomboids. The emissive properties of these bis(phosphine) organoplatinum metallacycles arise from ligand-centered transitions involving π-type molecular orbitals with modest contributions from metal-based atomic orbitals. The D_{2h} rhomboid self-assembled from 2,6-bis(4-pyridylethynyl)aniline and a 60° organoplatinum(II) acceptor has a low-energy excited state in the visible region and emits above 500 nm, properties which greatly differ from those of the parent 2,6-bis(4-pyridylethynyl)aniline ligand.

INTRODUCTION

A breadth of literature can be found on transition metal-mediated coordination-driven self-assembly, and over the past decade the development of this field has rapidly grown to include more complex synthetic designs and applications ranging from host–guest chemistry[1−17] and catalysis[18−25] to light harvesting.[26−31] The various design methodologies behind coordination-driven self-assembly developed by Cotton,[32,33] Fujita,[34,35] Hupp,[36,37] Mirkin,[38,39] Raymond,[40,41] Stang,[42] and others[43−45] have afforded a variety of discrete metallacycles and metallacages with well-defined shapes and sizes. Using a strategy dubbed the *directional-bonding approach*, the archetypal construction of these structures in the Stang laboratory utilizes bis(phosphine) Pt(II) metal nodes and pyridyl-based organic spacers wherein each component has encoded directionality and angularity which dictates the architectural outcome.[42,46−48] Maturation of this field has led to increasingly complex systems, with single-pot multicomponent systems[49−57] and postsynthetic modifications[58,59] being at the forefront of structural design. However, studies which probe the photophysical properties of supramolecular bis(phosphine) Pt(II) metal–organic structures, required to effectively develop bioimaging and sensing applications, are rare.

The use of discrete, metal–organic supramolecular structures in biological settings has garnered attention lately, primarily as vessels or capsules for the trafficking and delivery of therapeutic agents, biosensing, and bioimaging.[60−67] In addition, certain assemblies have demonstrated inherent drug activity, often due to the transition metal ions present in the structure. While reports for Pt(II)-based self-assemblies are very rare,[68] in the past few years, several reports have demonstrated that ruthenium-based metallacages show cytotoxicity toward cancerous cell lines *in vivo*.[69−78] However, little is known about the mechanism of uptake and release for these systems. The biological systems in which these supramolecular structures are used are complex, containing many ligands (e.g., amino acids, glutathione, etc.) that are capable of coordinating to a metal center and degrading the metal–organic structure. An *in vitro* study using several biological ligands and a cationic Ru(III) trigonal prism supports the previously proposed hypothesis that the cytotoxicity arises from degradation pathways.[80] While this study was insightful, the current paradigm of having to perform separate experiments to access information on cytotoxicity and the species giving rise to cytotoxicity is laborious, and systems that can streamline this process into a single experiment are attractive.

Monitoring structural integrity *in vivo*, cell uptake, localization, and cytotoxicity studies of a supramolecular assembly can be facilitated by using constructs with unique photophysical properties from their molecular components. One strategy to imbue emissive properties to a self-assembly is to tether a known fluorophore using common organic coupling techniques. The issue with such a design is that the emissive signature

Received: April 16, 2012
Published: June 12, 2012

   dx.doi.org/10.1021/ja3036515 | J. Am. Chem. Soc. 2012, 134, 10607−10620

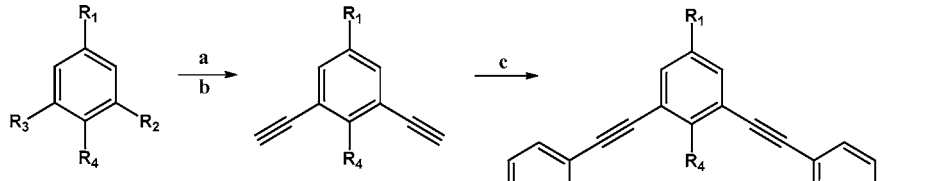

1: $R_1 = NH_2$, R_2 & R_3 = I, R_4 = H
2: R_1 = H, R_2 & R_3 = Br, $R_4 = NH_2$
3: $R_1 = NH_2$, R_4 = H
4: R_1 = H, $R_4 = NH_2$
5: $R_1 = NH_2$, R_4 = H (Exohedral Functionalized Ligand)
6: R_1 = H, $R_4 = NH_2$ (Endohedral Functionalized Ligand)
7: R_1 & R_4 = H (Non–Functionalized Ligand)

Figure 1. Ligand scaffolds employed for metallacycle synthesis. Conditions: (a) 10 mol % $Pd(PPH_3)_4$, 10 mol % CuI, acetylene-TMS, Et_3N, THF, 60 °C, 24 h; (b) KOH, MeOH, 24 h; (c) 10 mol % $Pd(PPH_3)_4$, 10 mol % CuI, 4-bromopyridine hydrochloride, Et_3N, THF, 60 °C, 24 h.

of the parent fluorophore-appended building block often matches that of the constructed assembly. Thus, it is impossible to distinguish between the self-assembly and decomposition products on the basis of emission alone, which is typically the handle used in the aforementioned biological applications. This problem is avoided by using systems in which the core of the final assembly is inherently emissive.

Mono- and multinuclear platinum complexes have been investigated thoroughly for their inherent photophysical properties and have exhibited low-energy absorption bands, long-lived and low-energy excited states, and high quantum yields.[81−101] These properties make a multinuclear Pt(II) self-assembled metallacycle an attractive target for the proposed application. Although the photophysics of mono- and multinuclear Pt(II) complexes have been investigated extensively, the photophysics of Pt-pyridyl metallacycles have largely been understudied.[102−104] One rare example is the study of rhomboids constructed with 1,2-bis(3-pyridyl)ethyne and 1,4-bis(3-pyridyl)-1,3-butadiyne using time-dependent density functional theory (TD-DFT) calculations.[105] The low-energy transitions of both rhomboids correspond to transitions between molecular orbitals that contain a large amount of ligand character. It was observed that increasing the size of the π-system by the addition of ethylene spacers within the ligand resulted in red-shifted emission of the rhomboids. Goodson et al. studied the ultrafast optical excitation and relaxation of a series of Pt-pyridyl rectangles and triangles.[106] It was determined that for self-assemblies with multiple platinum centers, increased amounts of intersystem crossing (ISC) occurred due to spin−orbit coupling. This "heavy-atom effect" manifested itself in decreased excited-state lifetimes, and since the triplet excited state was plagued by non-emissive decay pathways, low quantum yields were observed.

Recently, Pistolis et al. synthesized a boron dipyrromethene (BODIPY) Pt metallacycle whose emission was significantly red-shifted compared to that of the free ligand (λ_{em} = 592 versus 545 nm).[107] However, the quantum yield (Φ) of the metallacycle species was low compared to that of the ligand (6% versus 47%). When an ethylene spacer was added between the coordinating pyridyl units and the BODIPY backbone, the photophysical properties of the BODIPY ligand were conserved after coordination with the platinum acceptor. This study demonstrates the delicate balance between the isolation of the pyridyl-based ligand-centered electronic transitions and the bis(phosphine) platinum(II) metal center's ability to perturb the ligand-centered excited state. Too much Pt character and spin−orbit coupling open up non-radiative decay pathways; with too little, the emissive characteristics of the assembly do not differ enough from those of the building blocks to allow them to be distinguished from one another.

In an effort to synthesize a rhomboid-shaped metallacycle that could satisfy this careful balance, 4-ethynylpyridyl-based ligands with aniline core motifs were considered. Hooley et al.[108] recently reported the synthesis and photophysical characterization of 2,6-bis(pyridin-3-ylethynyl)aniline, which has Φ = 36% with a low-energy absorption band at 441 nm. Altering the 2,6-bis(pyridin-3-ylethynyl)aniline structure slightly, a highly emissive ligand with the correct angularity and directionality was synthesized for the construction of Pt(II)-incorporated metallacycles.

We now report the synthesis and characterization of a series of novel bis(pyridyl)aniline ligands and their use in the self-assembly of rhomboids. Steady-state absorption and fluorescence spectra were collected for each ligand and compared to those of their respective D_{2h} rhomboids synthesized with a 60° phenanthrene-based Pt acceptor. Rhomboids amine-functionalized in the interior (endohedral) and on the periphery (exohedral) were synthesized; however, only the endohedral aniline metallacycles displayed red-shifted emission compared to the free ligands. TD-DFT calculations were employed to probe the nature of the optical transitions for the rhomboids. Also, a hexagon was synthesized using a 180° organoplatinum(II) acceptor to investigate whether size or shape of 2-D metallacycles affects the photophysical properties. Herein, the synthesis, photophysical characterization, and quantum mechanical description of the electronic transitions are discussed for a series of metallacycles.

RESULTS

Ligand Synthesis and Photophysical Characterization.

The endohedral, exohedral, and non-functionalized[109] ligand scaffolds employed for metallacycle synthesis are shown in Figure 1. Each ligand contains three components: (1) a central ring with or without amino groups for electronic tuning of the ligand; (2) ethynyl spacers that are *meta* with respect to each other, which provides the requisite internal 120° angle for the synthesis of the D_{2h} rhomboids or D_{6h} hexagons; and (3) 4-pyridyl moieties at the periphery for metal complexation.

The exohedral and endohedral aniline-based ligands **5** and **6** were prepared stepwise using a Sonogashira coupling, deprotection, and second Sonogashira coupling. Ligand **6** was prepared in modest yields due to alternate reaction pathways, mainly uncontrollable indole formation from the *ortho* aniline acetylene core during the Pd-catalyzed 4-pyridyl insertion.[108]

dx.doi.org/10.1021/ja3036515 | J. Am. Chem. Soc. 2012, 134, 10607−10620

Ligand **8** was prepared in modest yield (58%) via a Suzuki cross-coupling of **2** with 4-bromopyridine HCl (Figure 2).

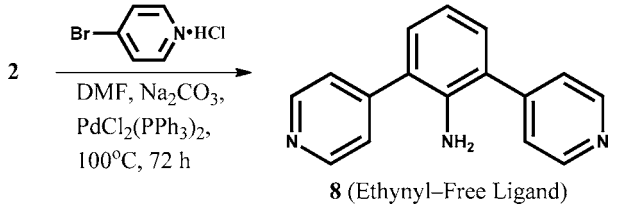

Figure 2. Preparation of ligand **8** via a Suzuki cross-coupling of **2** and 4-bromopyridine HCl.

The absorption profiles of each of the four ligands **5**, **6**, **7**, and **8** are shown in Figure 3 (left). Ligand **7** has two sharp absorption bands at 282 and 300 nm with extinction coefficients (ε) of 52 000 and 45 900 $cm^{-1}\,M^{-1}$, respectively. These bands are present in both **5** and **6**, but with decreased intensity (see Table 1). **5** and **6** have broad, lower-energy absorption bands at 347 and 373 nm which are not present in **7**. These two absorption bands have ε = 5500 and 13 700 $cm^{-1}\,M^{-1}$, respectively. Ligand **8** does not maintain the two higher-energy absorption bands (found at 282 and 300 nm) that are present in **5**, **6**, and **7**, although it does possess a broad absorption band centered at 329 nm with ε = 5000 $cm^{-1}\,M^{-1}$.

The emission spectra (Figure 3, right) for **5**, **6**, and **8** all show similar single, broad bands with λ_{max} = 389, 420, and 397 nm, respectively. The quantum yields of **5**, **6**, and **8** are 41, 65, and 34%, respectively. Ligand **7** was determined to be weakly emissive (Φ = 8.4%), with a sharp band centered at 347 nm and a broad band at 364 nm with a shoulder at 392 nm.

Metallacycle Synthesis and Photophysical Characterization. *Rhomboids 10–12.* Rhomboids **10**, **11**, and **12**, shown in Figure 4, were prepared by treating CH_2Cl_2 solutions of organoplatinum acceptor **9** with **5**, **6**, and **7**, respectively, in a 1:1 ratio. After 24 h of stirring at room temperature, the rhomboids were precipitated out of solution using diethyl ether, isolated, and re-dissolved in CD_2Cl_2. The final products were characterized by ^1H and $^{31}P\{^1H\}$ NMR and electrospray ionization mass spectrometry (ESI-MS). In each $^{31}P\{^1H\}$ NMR spectrum of **10**, **11**, and **12**, an intense singlet with concomitant ^{195}Pt satellites was observed (see Supporting Information), indicating that all the phosphorus atoms in solution were equivalent. The $^{31}P\{^1H\}$ NMR of rhomboid **11** is shown in Figure 5. A singlet at δ = 12.61 ppm with the Pt satellites ($^1J_{Pt-P}$ = 2684 Hz) was observed. Also, the expected downfield shifts of the α- and β-pyridyl protons upon coordination to the platinum were observed in the ^1H spectrum, consistent with previous observations of Pt-based metallacycles and cages.[53,110−112] As shown in Figure 5, the α- and β-protons on the pyridyl ring are split into two sets of two doublets upon coordination. The H_α-Py of **6**, shown in red at δ = 8.62 ppm, is split into two doublets at δ = 8.89 and 8.69 ppm, while the H_β-Py of **6**, shown in blue at δ = 7.38, is split into two doublets at δ = 8.28 and 7.76 ppm. Isotopically resolved peaks for two of the charge states for **10**−**12** (see Supporting Information) from the loss of nitrate counterions in the ESI-MS spectra further support the formation of a single, discrete rhomboid. Isotopically resolved signals for $[\mathbf{11}\text{-}2ONO_2]^{2+}$ and $[\mathbf{11}\text{-}3ONO_2]^{3+}$ are shown in Figure 6.

Figure 7 (left) displays the absorption profiles for rhomboids **10**, **11**, and **12**. Each of the rhomboids has two high-energy absorption bands centered at 258 and 267 nm. Interestingly, **11** has a higher extinction coefficient for the 258 nm band (ε = 135 000 $cm^{-1}\,M^{-1}$) with respect to the 267 nm band (ε = 130 000 $cm^{-1}\,M^{-1}$), while the converse is observed for **12**; it has a higher extinction coefficient for the 267 nm band (ε = 79 900 $cm^{-1}\,M^{-1}$) than the 258 nm band (ε = 73 600 $cm^{-1}\,M^{-1}$). It should be noted that the overall intensity of both bands decreases from **12** to **10**. Assemblies **10**, **11**, and **12** all have an absorption band centered at 288 nm, with ε = 77 500, 85 200, and 69 900 $cm^{-1}\,M^{-1}$, respectively. Both **10** and **12** have two absorption bands centered at 288 and 306 nm, while **11** has a single, broad absorption band centered at 317 nm. There is a weak shoulder for **12** centered at 356 nm, with ε = 10 200 $cm^{-1}\,M^{-1}$. For metallarhomoid **10**, there is a weak, broad absorption band centered at 370 nm, with ε = 20 100 $cm^{-1}\,M^{-1}$. **11** has the lowest energy absorption band of the three rhomboids, with a band centered at 430 nm. This absorption band also has the highest extinction coefficient (ε = 39 900 $cm^{-1}\,M^{-1}$) of the lowest energy absorption bands for **10**−**12**.

Figure 7 displays the emission profiles for **10** and **11**, with both rhomboids having a single, broad emission band centered at 400 and 522 nm, respectively. The quantum yields of **10** and **11** are 4.0 and 28%, respectively. The emission profile for **12** is not shown because the quantum yield was too low.

Rhomboid 13. The synthesis of **13** was accomplished by stirring **8** and **9** in a 1:1 ratio in MeOH at a temperature of 55 °C for 24 h. Diethyl ether was added to the brightly colored, green solution to precipitate the product. The product was then

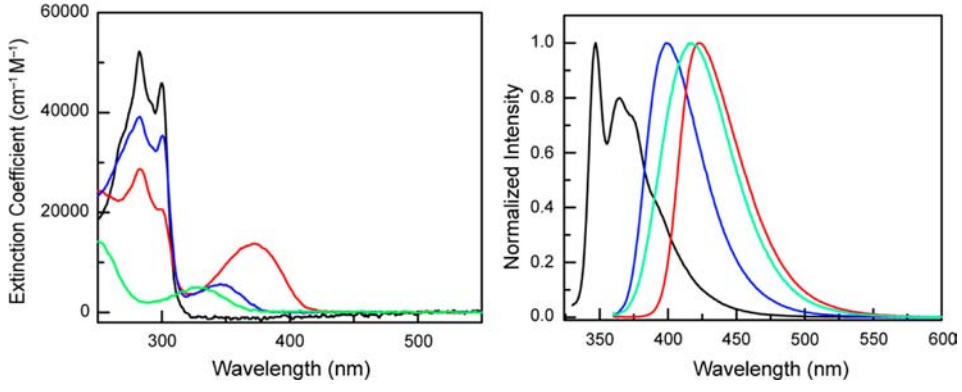

Figure 3. Absorption (left) and emission (right) profiles for ligands **5** (blue), **6** (red), **7** (black), and **8** (cyan). The spectra were collected using a 1 cm path length in aerated methylene chloride.

dx.doi.org/10.1021/ja3036515 | J. Am. Chem. Soc. 2012, 134, 10607−10620

Table 1. Extinction Coefficients, λ_{emiss}, and Quantum Yield for Each Ligand and Self-Assembly

compd	description	absorption bands λ_{max}/nm [$\varepsilon \times 10^3$/cm^{-1} M^{-1}]	λ_{exc}/nm	λ_{emis}/nm	Φ/%[a]
5	exohedral aniline ligand	282 [39.0], 300 [35.3], 347 [5.50]	356	399	41
6	endohedral aniline ligand	282 [28.6], 300 sh [20.7], 373 [13.7]	356	422	65
7	non-functionalized ligand	282 [52.0], 300 [45.9]	324	347, 364, 392 sh	8.4
8	ethynyl-free ligand	329 [5.00]	356	417	34
10	exohedral functionalized rhomboid	258 sh [100], 267 [103], 288 [77.5], 306 [86.6], 319 [91.2], 370 sh [20.1]	356	400	4.0
11	endohedral functionalized rhomboid	258 [135], 267 sh [130], 288 [85.2], 317 [112], 430 [39.9]	430	522	28
12	non-functionalized rhomboid	258 sh [73.6], 267 [79.9], 288 [69.9], 306 [95.3], 319 [98.5], 356 sh [10.2]	356	no emiss[b]	—
13	ethynyl-free rhomboid	285 [167], 314 sh [76.3], 385 [37.8]	385	493	3.7
14	endohedral functionalized hexagon	284 sh [95.2], 318 [139], 422 [87.6]	422	505	15

[a]Quinine sulfate and anthracene were used as standards for quantum yield determination. [b]A very weak emission profile was obtained with a signal-to-noise ratio unsuitable for quantum yield determination.

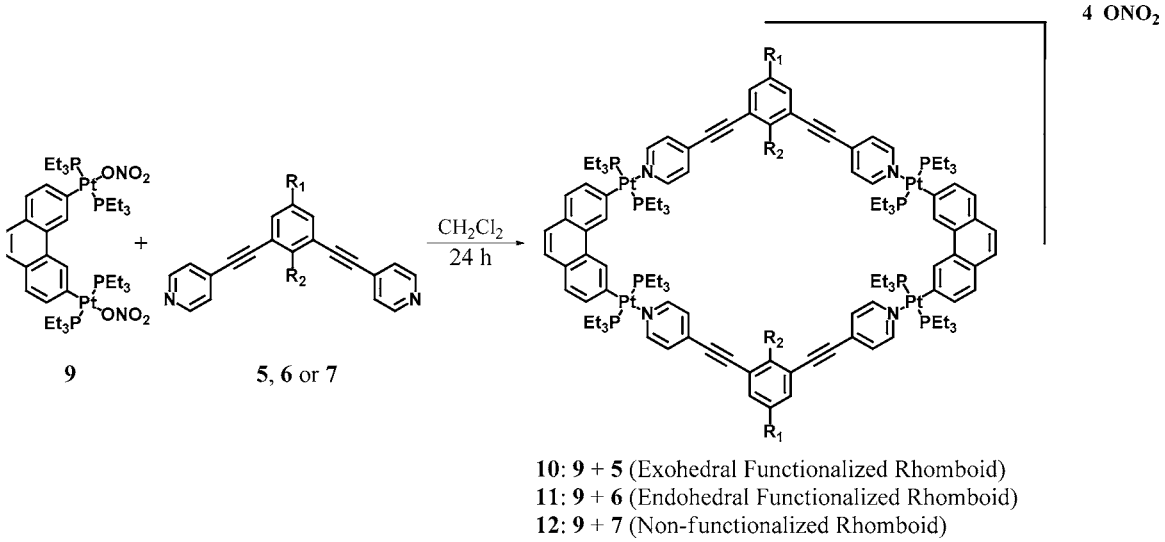

Figure 4. Solutions of **9** with **5**, **6**, or **7** are stirred in a 1:1 stoichiometric fashion in CH_2Cl_2 for 24 h to afford D_{2h} rhomboids **10**, **11**, and **12**.

isolated and re-dissolved in CD_2Cl_2 for characterization (see Supporting Information).

Figure 9 displays the absorption and emission profiles for rhomboid **13**. In the absorption spectrum there is an intense, high-energy absorption band centered at 285 nm, with ε = 167 000 cm^{-1} M^{-1}. This band has a shoulder at 314 nm (ε = 76 300 cm^{-1} M^{-1}). A broad, low-energy absorption band appears at 385 nm, with ε = 37800 cm^{-1} M^{-1}. Within this broad band there are two optical transitions that overlap and have slightly higher extinction coefficients, at 344 and 362 nm.

Hexagon 14. Hexagon **14** was synthesized by weighing 180° acceptor **15** and ligand **11** into separate vials and dissolving both with methylene chloride (Figure 10). The clear solution containing **15** was then added dropwise to the yellow solution of **11**. The resulting brightly colored, green solution was then allowed to stir for 24 h at room temperature. The product was then precipitated with diethyl ether, isolated, and re-dissolved in CD_2Cl_2 for characterization (see Supporting Information). It should be noted that if both compounds are weighed into the same vial and dissolved together, a low yield will be obtained due to insoluble kinetic byproducts. Parent ions of the hexagon structure were not observed in the ESI spectra (both ToF and FT-ICR detectors were utilized with and without acid) due to fragmentation; however, several unique fragments were observed that support the formation of the hexagonal structure when analyzed in conjunction with the NMR spectra (see Supporting Information).

Figure 11 displays the absorption and emission profiles for **14**. The absorption spectrum displays a high-energy, sharp band centered at 318 nm, with a shoulder at 284 nm, while a lower-energy broad band is centered at 422 nm. The two higher-energy bands have extinction coefficients of 139 000 and 95 200 cm^{-1} M^{-1}, respectively, while the lower-energy band has an extinction coefficient of 87 600 cm^{-1} M^{-1}. The emission profile of **14** (dashed) has a single, broad band centered at 505 nm, and **14** has Φ = 15%.

DISCUSSION

Ligands. The photophysical properties of aniline have been widely studied. In general, intense absorption bands for aniline are due to $\pi \rightarrow \pi^*$ transitions.[113−116] Typically, there are two electronic transitions that correspond to the $S_0 \rightarrow S_1$ and $S_0 \rightarrow S_2$ excited states, with both transitions being red-shifted for larger arene−aniline systems. For simple anilines, the main pathway for non-radiative decay is ISC from the S_1 to T_1 state, wherein the $T_1 \rightarrow S_0$ conversion does not phosphoresce.[113] For larger arene−anilines the rate constant for ISC is smaller, which leads to higher quantum yields.[117]

Ligands **5**, **6**, and **7** follow a similar trend, where two excited states S_1 and S_2 are modulated by the presence and position of the aniline amine. For **7**, we assign the $S_0 \rightarrow S_1$ transition to the

dx.doi.org/10.1021/ja3036515 | J. Am. Chem. Soc. 2012, 134, 10607−10620

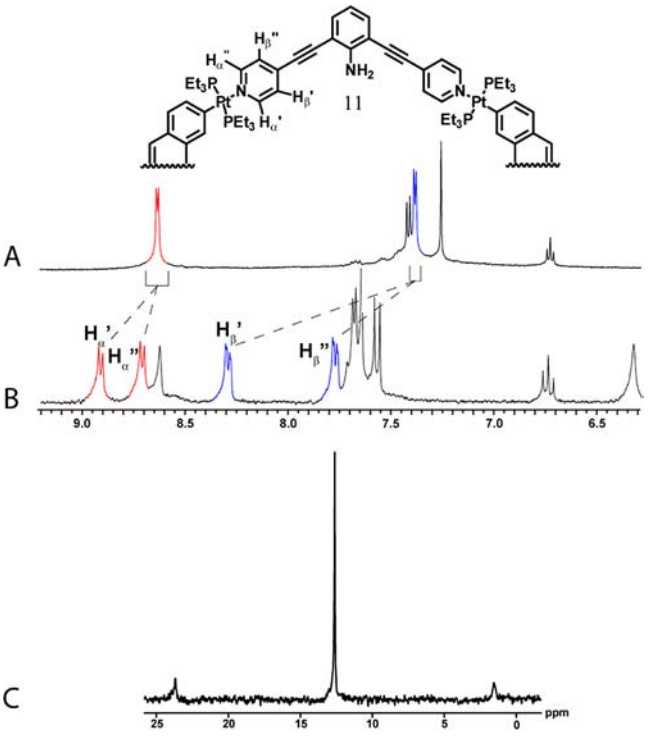

Figure 5. (A) ^{1}H NMR spectra for **6**, with the α- and β-pyridyl proton signals colored in red and blue. (B) ^{1}H NMR spectra for **11**, demonstrating the downfield shift and splitting of the α- and β-protons on the pyridyl ring upon metal complexation. (C) ^{31}P{^{1}H} spectrum for **11**.

lower-energy band at 300 nm. Decay from this state appears to be significantly non-radiative compared to the other aniline-based ligands, which is supported by the lower quantum yield for **7** (Φ = 8.4%) with respect to **5** (Φ = 41%) and **6** (Φ = 65%). The major pathway for non-radiative decay is believed to be through ISC, followed by a non-emissive $T_1 \rightarrow S_0$ transition. The S_1 excited state for **5** and **6** is lower in energy than that of **7**, while the S_2 state (300 nm) is similar in energy to that of the S_1 state for **7** (300 nm); it is possible that a lower-energy, electronically forbidden state exists for **7**. The variation in quantum yield between **5**, **6**, and **7** may be rationalized by considering these two excited states. If the emissive singlet state, which is S_2 in compound **7**, is stabilized in compounds **5** and **6**, it may be stabilized and approach the S_1 state. This stabilization makes it populated upon excitation of **5** and **6**, leading ultimately to increased emission since ISC is attenuated. Evidence for this claim comes from the observed quantum yields for **5** (Φ = 41%) and **6** (Φ = 65%), as well as absorption features among the series of compounds. The trend for the band centered at 300 nm to decrease with the growing lower-energy bands of **5** (347 nm) and **6** (373 nm) suggests that an intimate relationship between these two electronic transitions exists. The lack of electronic transitions at 282 and 300 nm in **8** provides evidence linking the two transitions to the presence of the ethynyl moieties.

The lower-energy excited state of **6** compared to **5** can be attributed to the position of the amine group on the central ring. The amine in **5** is *meta* to the ethynyl moieties, and while the lone pair on the amine nitrogen is not in direct resonance with the ethynyl moieties, the σ_{meta} value is negative (−0.16).[118] However, when the amine is *ortho* to the ethynyl moieties, it is in direct resonance, lowering the energy of the excited state of **6**. This is manifested in a 23 nm red-shift of the emission of **6** relative to **5**.

Compound **8** lacks the ethynyl moieties responsible for absorption bands at 282 and 300 nm. It does have a lower-energy broad absorption band centered at 329 nm; however, it is blue-shifted compared to those observed for **5** (347 nm) and **6** (373 nm). This blue-shift is attributed to the smaller π-system present in the ethynyl-free ligand. Interestingly though, the ethynyl spacer does not seem to have a significant effect on the emission spectra. When comparing the lowest-energy absorption bands between **6** (373 nm) and **8** (329 nm), there is a 44 nm red-shift; however, a 5 nm red-shift is observed between the emission spectra. This indicates that the excited state from which the radiative pathway decays is similar in energy to that of **6**, despite being a higher-energy transition. Moreover, the

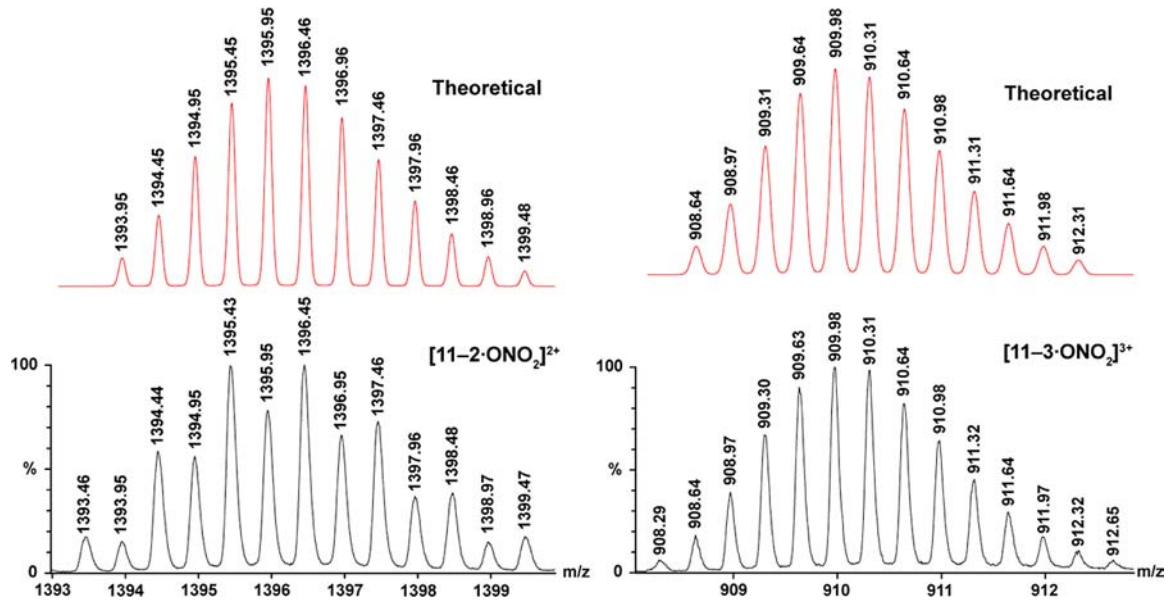

Figure 6. ESI-MS spectra of [**11**-2ONO$_2$]$^{2+}$ and [**11**-3ONO$_2$]$^{3+}$ (black) and simulated spectra (red).

dx.doi.org/10.1021/ja3036515 | J. Am. Chem. Soc. 2012, 134, 10607−10620

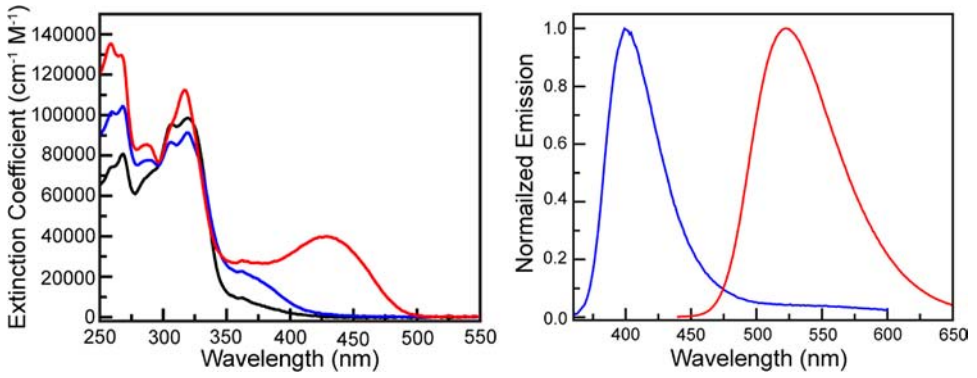

Figure 7. Absorption (left) and emission (right) profiles for **10** (blue), **11** (red), and **12** (black). Spectra were recorded in aerated CH_2Cl_2.

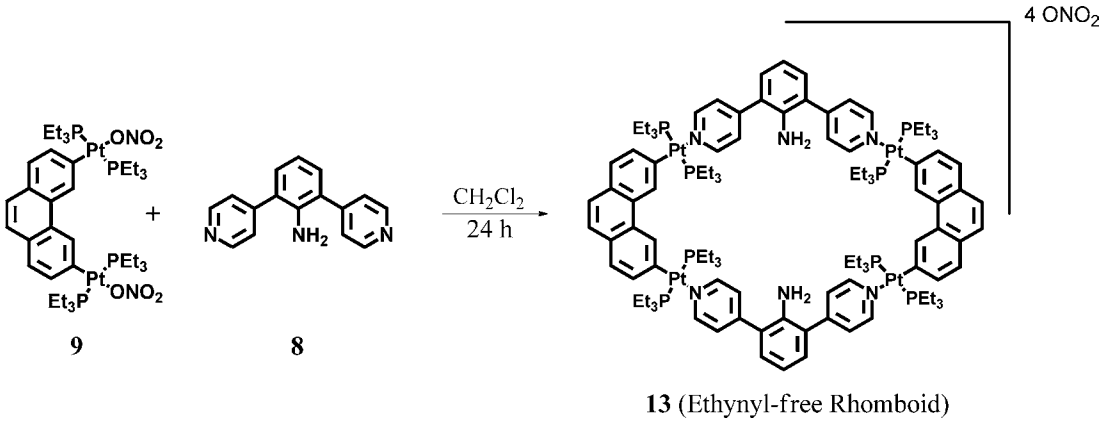

Figure 8. Compounds **9** and **8** are stirred in a 1:1 stoichiometric fashion in CH_2Cl_2 for 24 h to afford **13**.

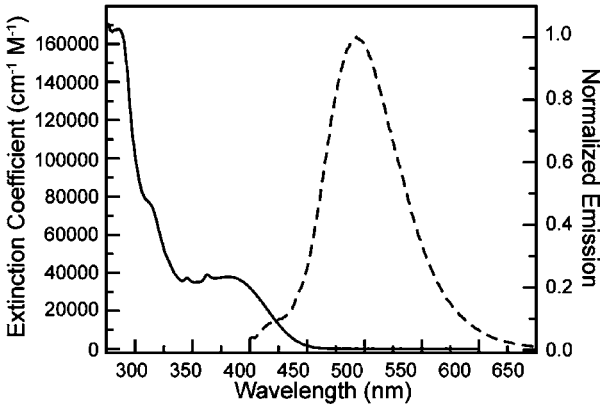

Figure 9. Absorption (solid) and emission (dashed) profiles for **13**. The spectra were collected using 1 cm path length in aerated CH_2Cl_2.

quantum yield of **8** is almost half that of **6**, providing evidence that the excited state has a much lower rate constant for the radiative pathway. The major component for the non-radiative pathway could be attributed to ISC, as a similar phenomenon has been observed with simple aniline compounds (i.e., a smaller π-system has a higher rate constant for ISC).

Self-Assemblies. In all cases, the self-assemblies have red-shifted lower-energy absorption bands and lower quantum yields than their constituent ligands. However, only self-assemblies constructed using endohedral aniline ligands **11**, **13**, and **14** displayed appreciable red-shifts in the emission spectra when compared to endohedral aniline ligands **6** and **8**. A 17 nm blue-shift was observed for **14** when compared to **11**. Each of these observed results will be addressed individually.

When comparing the ligands and their respective self-assemblies, a red-shift was observed for the lower-energy electronic transitions. For example, the lowest-energy electronic transition for endohedral aniline ligand **6** is centered at 373 nm, while the self-assemblies constructed from this ligand, **11** and **14**, have bands centered at 430 and 422 nm. This phenomenon was attributed to the metal center coordinating with the pyridyl nitrogen and perturbing the electronic structure of the ligand. As will be shown in the TD-DFT section, the molecular orbitals involved with the electronic transitions are of π-type symmetry. Therefore, it is hypothesized that π-backbonding from the metal center to the nitrogen π^* enriches the ligand π-system and lowers the energy required for excitation.

The quantum yield of each self-assembly is lower than the quantum yields of the ligands from which they are constructed. As previously discussed, aniline undergoes $S_1 \rightarrow T_1$ ISC and then non-radiatively decays back to the ground state, S_0. Heavy atoms are known to enhance the rate of spin-forbidden processes such as ISC. Therefore, inclusion of platinum metal centers in the self-assemblies will increase the rate constant for ISC for the ligand-centered transitions. This manifests itself in the quantum yield being lower in the self-assembly than in the ligand used for its construction. For example, **8** has Φ = 8.4%, while **12** is non-emissive. In a more impressive example, **5** has Φ = 41%, while **10** has Φ = 4.0%.

Interestingly, the exohedral aniline ligand **5** and **10** have similar λ_{max} for emission, 399 and 400 nm, despite **10** having a lower-energy absorption band than **5** (370 versus 347 nm).

dx.doi.org/10.1021/ja3036515 | J. Am. Chem. Soc. 2012, 134, 10607−10620

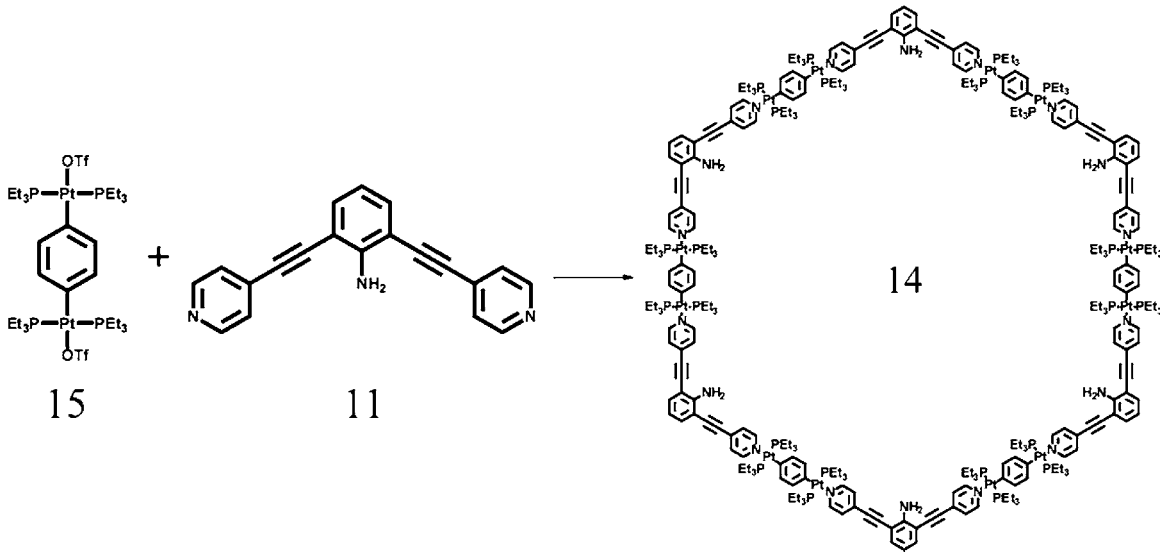

Figure 10. Solutions of **15** and **11** were prepared using CH_2Cl_2. **15** was then added dropwise to a solution of **11** and the mixture stirred for 24 h to afford **14**.

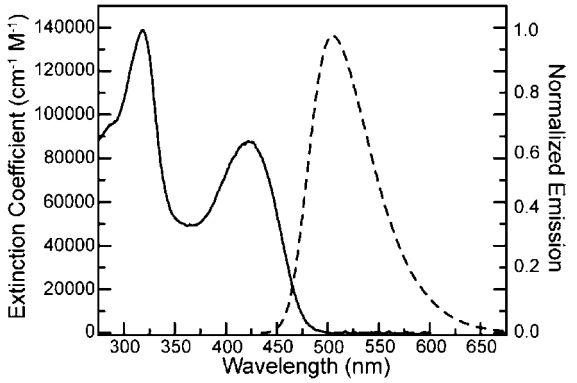

Figure 11. Absorption (solid) and emission (dashed) profiles for **14**. The spectra were collected using 1 cm path length in aerated CH_2Cl_2.

This implies that **5** and **10** have ligand-centered excited states with similar energies.

Unlike **10**, self-assemblies constructed using endohedral aniline ligands **11**, **13**, and **14** displayed appreciable red-shifts in the emission spectra when compared to endohedral aniline ligands **6** and **8**; however, **15** has an emission profile similar to that of ligand **5**. The low-energy optical transition for **11** in the absorption spectrum is 430 nm, and the λ_{max} for emission is 522 nm, while **13** has a low-energy absorption band of 385 nm and a λ_{max} for emission of 493 nm. This trend is continued for **14**, which has a low-energy absorption band of 422, while the λ_{max} for emission is 505 nm.

A 17 nm blue-shift in the emission spectrum for **14** was observed compared to **11**. While organoplatinum(II) acceptor **15** is different than **9** and could account for this difference in the emission spectra, the purpose of making a larger self-assembly was to determine whether the photophysical properties and shape or size of the metallacycle were intimately related. By increasing the size of the metallacycle, there was only a small blue-shift of 8 nm in the lower-energy absorption band, which could be attributed to the difference between **15** and **9**. Also, the extinction coefficient of this lower-energy band is higher in **14** (ε = 87 600 $cm^{-1}\,M^{-1}$) than in **11** (ε = 39 900 $cm^{-1}\,M^{-1}$). This is to be expected if each metallacycle consists of multiple localized π-systems; however, it does not manifest itself as a strictly linear relationship when comparing the extinction coefficients for **14** and **11**. This does implicate, though, that the self-assembly's inherent photophysical properties are ligand centered. This is evidence that, for Pt-based constructs of this type, the specific ligands used in a given self-assembly have a larger influence on the photophysical properties than the particular size or shape of the assembly.

DFT and TD-DFT General Information. Single-point calculations were performed using a split basis set, where Becke three-parameter hybrid exchange, the Lee−Yang−Parr correlation functional (B3LYP),[119,120] and the 6-31G** basis set[121] were used for C, H, N, and P atoms, while the Los Alamos National Laboratories (LANL2DZ)[122] basis set and pseudopotential were used for Pt. To minimize computational cost, PH_3 ligands were utilized instead of PEt_3; therefore, the model used to approximate self-assembly **10** will be termed **10**-PH_3.

Table 2. Wavelength, Molecular Orbitals Involved, Oscillator Strength, and Description for Each of the Three Electronic Transitions Predicted for 11-PH_3

wavelength/nm	orbital transitions		oscillator strength, f	description
458.3	349 → 354	HOMO−3 → LUMO+1	1.1438	loss of e^- density on aniline nitrogen ethynyl $^1\pi \rightarrow {}^1\pi^*$
	350 → 353	HOMO−2 → LUMO		
353.4	345 → 356	HOMO−7 → LUMO+3	2.3945	e^- density increases on aniline nitrogen ethynyl $^1\pi \rightarrow {}^1\pi^*$
	346 → 355	HOMO−6 → LUMO+2		
343.0	345 → 353	HOMO−7 → LUMO	0.8230	ethynyl $^1\pi \rightarrow {}^1\pi^*$
	346 → 354	HOMO−6 → LUMO+1		

dx.doi.org/10.1021/ja3036515 | J. Am. Chem. Soc. 2012, 134, 10607−10620

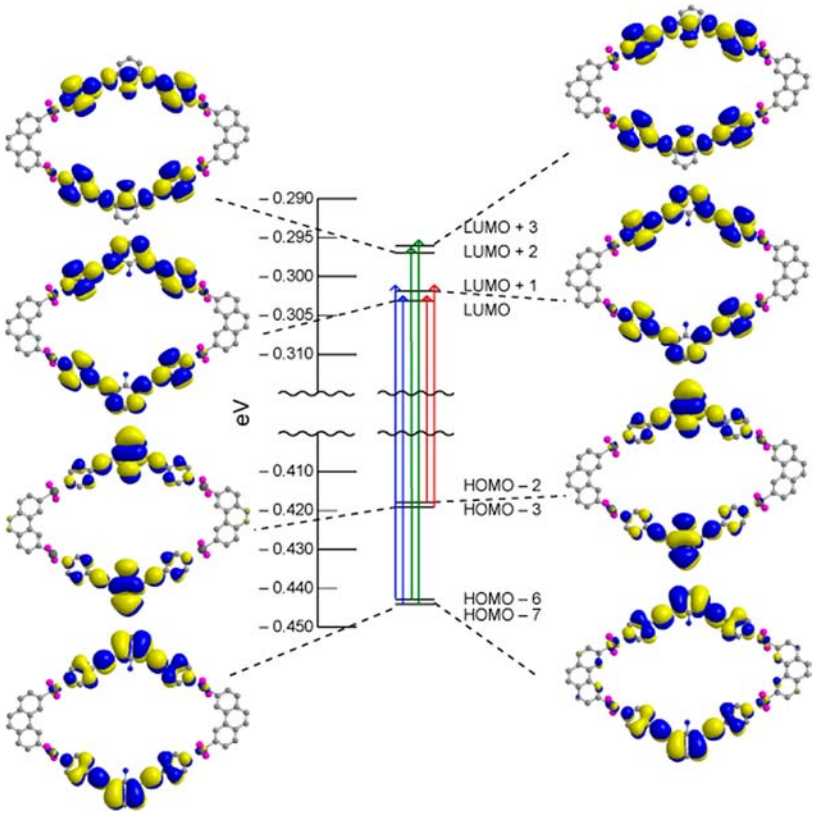

Figure 12. Predicted TD-DFT transitions for a rhomboid model with oscillator strengths above 0.3. Three excited states are predicted, corresponding to absorptions at 458.3 (red), 353.4 (green), and 343.0 nm (blue).

This nomenclature was applied to all models. The vertical singlet transition energies of the complexes were computed at the TD-DFT level within G09[123] using the ground-state optimized structure. For the structures that were calculated, 1486−1598 molecular orbitals were observed, and each molecular orbital number that is listed is real and in its absolute energetic order. The nomenclature that will be utilized to discuss these molecular orbitals will be relative to the HOMO and LUMO (i.e., HOMO−1 is the molecular orbital directly below the HOMO).

TD-DFT Results and Discussion. *Rhomboid 11.* For endohedral aniline rhomboid **11**-PH_3, Table 2 lists the wavelengths for the theoretical electronic transitions that have oscillator strengths over 0.3 from the output of the TD-DFT calculation. For each electronic transition at a particular energy, the following are listed: the orbitals associated with that transition, the oscillator strength, and a general description of the changes between the ground-state and excited-state molecular orbitals involved in the transition.

Each molecular orbital has π-type symmetry and two regions of electron density that are ligand-centered and separated by the phenanthrene moieties of the organoplatinum(II) units on the D_{2h} rhomboid. Rhomboid **11** has three predicted optical transitions, at 458.3, 353.4, and 343.0 nm, with oscillator strengths of 1.1438, 2.3945, and 0.8230, respectively (see Table 2). All three predicted transitions involve filled molecular orbitals with bonding character between the carbons of the ethynyl moieties. The corresponding virtual or unoccupied molecular orbitals have antibonding character between the carbon atoms in the ethynyl moieties, which leads to a weakening of the π-system on the ethynyl moiety during the electronic transition. This transition is ascribed as $^1\pi \rightarrow {}^1\pi^*$. Both transitions at 353.4 and 343.0 nm originate from low-lying (HOMO−6 and HOMO−7) occupied molecular orbitals. The molecular orbitals for the lowest-energy transition at 458.3 nm have electron density on the central aniline amine group which is not present in the corresponding virtual molecular orbitals. The opposite is observed for the electronic transition at 353.4 nm, where the occupied molecular orbitals have electron density on the central aniline amine group, while the unoccupied orbitals have significantly less.

Figure 12 displays the predicted electronic transitions and the molecular orbitals involved. After comparing the energies of the eight molecular orbitals involved in the three theoretical optical transitions, it was observed that there are four subsets of grouped molecular orbitals, with each subset consisting of two molecular orbitals that are close in energy. Moreover, each electronic transition consists of one energetically similar occupied ground-state "pair" going to an unoccupied excited-state "pair". These two energetically similar molecular orbitals are thought to be degenerate, as discussed below.

Rhomboid **11**-PH_3 has D_{2h} symmetry, and each molecular orbital has two regions of electron density with π-symmetry. HOMO−7 and HOMO−6 contain a homologous ligand-centered π-system that is separated from the second ligand-centered π-system by the phenanthrene moiety on the Pt acceptor **9**. The second π-system is either identical to the localized π-system across from it (HOMO−7) or inverted (HOMO−6), which results in a change in the overall orbital symmetry.

Performing a population analysis on each molecular orbital corroborated the experimental conclusion that the optical transitions arise from ligand-centered transitions; it was calculated that over 96% of the electron density resides on

dx.doi.org/10.1021/ja3036515 | J. Am. Chem. Soc. 2012, 134, 10607−10620

Table 3. Wavelength, Molecular Orbitals Involved, Oscillator Strength, and Description for Each of the Two Electronic Transitions Predicted for 10-PH_3 and the Three Predicted for 12-PH_3

compd	wavelength/nm	orbital transitions		oscillator strength, f	description
10-PH_3	361.5	345 → 356	HOMO−7 → LUMO+3	2.4633	increase of e^- density on aniline nitrogen ethynyl $^1\pi \rightarrow {}^1\pi^*$
		346 → 355	HOMO−6 → LUMO+2		
	345.8	345 → 353	HOMO−7 → LUMO	0.7839	ethynyl $^1\pi \rightarrow {}^1\pi^*$
		346 → 354	HOMO−6 → LUMO+1		
12-PH_3	361.2	337 → 346	HOMO−7 → LUMO+1	1.5737	ethynyl $^1\pi \rightarrow {}^1\pi^*$
		339 → 348	HOMO−5 → LUMO+3		
		340 → 347	HOMO−4 → LUMO+2		
	342.6	339 → 345	HOMO−5 → LUMO	0.6351	ethynyl $^1\pi \rightarrow {}^1\pi^*$
		340 → 346	HOMO−4 → LUMO+1		
	338.7	335 → 345	HOMO−9 → LUMO	2.5610	ethynyl $^1\pi \rightarrow {}^1\pi^*$ charge transfer from phenanthrene to ligand
		337 → 346	HOMO−7 → LUMO+1		
		338 → 345	HOMO−6 → LUMO		
		340 → 347	HOMO−4 → LUMO+2		

ligand-based orbitals. That said, the inclusion of Pt afforded new photophysical properties relative to those of the free ligands. This implies that the metal center perturbs the electronic structure of the ligands. Since each molecular orbital is of π-type symmetry and extends onto the Pt metal center, it is hypothesized that π-backbonding from Pt to the pyridyl nitrogen π^* could be stabilizing the ligand-centered excited state, thus giving rise to the red-shifted absorption and emission bands.

The emission profile for **11** has a broad band centered at 522 nm, while **10** has a band centered at 400 nm. The difference in emission wavelength maxima was previously discussed and attributed to the difference in the σ values and resonance structures. Further analysis of the molecular orbitals determined that the unique positioning of the aniline nitrogen *ortho* to both ethynyl moieties allows for direct "bridging" of the two π-systems. This can be seen in molecular orbitals HOMO−3 and HOMO−2, where the p-orbital of the aniline nitrogen is in phase with the ethynyl π-system. This allows for the electrons in the p-orbital on the aniline nitrogen to participate in the π-system on the ethynyl moieties without having to traverse the central benzene ring, resulting in the large red-shift observed.

It should be noted that between molecular orbitals 352 (HOMO) and 353 (LUMO) there is a considerable amount of charge transfer from the metal acceptor unit and ligand; the organo-Pt(II) acceptor unit includes orbital contributions from the platinum, phenanthrene, and phosphine. In the HOMO, 98.12% of the electron density resides on the metal acceptor, while in the LUMO there is only 2.44 (for the ligand, 0.88% in the HOMO and 97.33% in the LUMO).

*Rhomboid **10** and **12**.* The exohedral aniline rhomboid model **10**-PH_3 has two predicted electronic transitions, at 361.53 and 345.8 nm, with oscillator strengths of 2.4633 and 0.7839 (see Table 3). The orbitals utilized in both transitions are deep, low-lying HOMO−6 and HOMO−7 orbitals, and for both electronic transitions, the electron is promoted to low-lying LUMO orbitals.

The occupied molecular orbitals HOMO−7 and HOMO−6 involved with the electronic transition at 361.5 nm have carbons that are bonding in the ethynyl moieties, while the unoccupied destination molecular orbitals LUMO+3 and LUMO+2 have carbons that are antibonding within the ethynyl moieties. This transition is ascribed as $^1\pi \rightarrow {}^1\pi^*$. Also, HOMO−7 and HOMO−6 have little electron density on the aniline nitrogen, but some electron density is present in the unoccupied molecular orbitals LUMO+2 and LUMO+3. This implies that the aniline amine is actively participating in the electronic transitions, even though it is meta to the ethynyl moieties.

The electronic transition at 345.8 nm has an oscillator strength of 0.7839 and is comprised of two molecular orbital transitions (HOMO−7 → LUMO and HOMO−6 → LUMO +1). Occupied molecular orbitals HOMO−7 and HOMO−6 both have the carbons in the ethynyl moieties bonding, while the destination unoccupied molecular orbitals have the carbons in the ethynyl moieties antibonding ($^1\pi \rightarrow {}^1\pi^*$). Therefore, the ethynyl moieties seem to be critical to the observed photophysical properties.

Rhomboid **10**-PH_3 also displays a significant amount of charge transfer between the 352 (HOMO) and 353 (LUMO) molecular orbitals. Molecular orbital 352 has 88.73% of the electron density residing on the organo-Pt(II) acceptor unit, with 10.08% on the ligand, while molecular orbital 353 has 2.68% on the organo-Pt(II) acceptor unit and 96.96% on the ligand.

Rhomboid **12**-PH_3 has three predicted electronic transitions, at 361.2, 342.6, and 338.7 nm, with oscillator strengths of 1.5737, 0.6351, and 2.5610 (see Table 3). The electronic transitions at 361.2 and 342.6 nm both correspond to a weakening of the ethynyl moieties ($^1\pi \rightarrow {}^1\pi^*$). It was predicted that **12** would have a higher-energy electronic transition centered at 338.7 nm that utilizes deep, low-lying HOMO−9 and HOMO−7 molecular orbitals, wherein the ethynyl moieties ($^1\pi \rightarrow {}^1\pi^*$) are weakened and a phenanthrene (acceptor)-to-ligand charge transfer occurs. After performing a population analysis on the molecular orbitals associated with this charge transfer, it was determined that 41% of electron density on the phenanthrene moiety of acceptor **9** moiety is transferred to **5**.

It should be noted that there is a considerable amount of charge transfer from the metal acceptor unit and ligand between molecular orbitals 344 (HOMO) and 345 (LUMO) for rhomboid **12**. Molecular orbital 344 has 96.63% of the electron density residing on the organo-Pt(II) acceptor unit, while in molecular orbital 345 there is only 2.20 (for the ligand, 0.43% in HOMO and 95.64% in the LUMO).

The experimental absorption spectra for **12** and **10** are shown in Figure 13, with the predicted lower-energy electronic transition for **10**-PH_3 overlaid. The theoretical lowest-energy electronic transition for **10**-PH_3 (361.53 nm) closely matches

dx.doi.org/10.1021/ja3036515 | J. Am. Chem. Soc. 2012, 134, 10607−10620

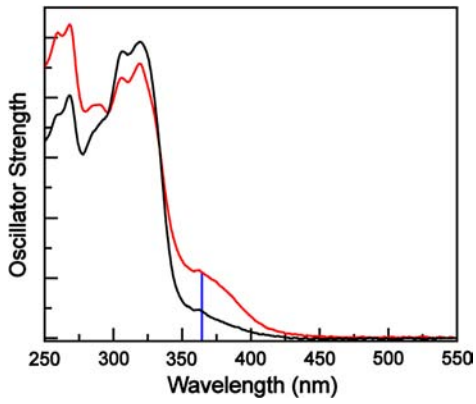

Figure 13. Experimental absorption spectra of **12** (black) and **10** (red) with the predicted optical transition at 361 nm (blue) overlaid.

the experimentally observed wavelength maximum for the low-energy absorption band, 370 nm. Also, the lowest-energy electronic transition for **12**-PH_3 was predicted to be centered at 361.2 nm, while it was experimentally observed at 356 nm. The theoretical oscillator strengths, which are related to the extinction coefficients, for **10**-PH_3 and **12**-PH_3 follow what is observed experimentally, with **10** having a larger extinction coefficient, at 361 nm, than that of **12**.

Rhomboid ***13***. Unlike rhomboids **10**-PH_3, **11**-PH_3, and **12**-PH_3, rhomboid **13**-PH_3 has C_{2v} symmetry. Rhomboid **13**-PH_3 was predicted to have a single electronic transition, at 378.2 nm, with an oscillator strength of 0.5194 (see Table 4). Both occupied molecular orbitals HOMO−5 and HOMO−4 have electron density centered on the central aniline core with density on the nitrogen, while the unoccupied molecular orbitals LUMO+1 and LUMO have little electron density on the aniline nitrogen. Moreover, the unoccupied molecular orbitals have more electron density displaced on the pyridyl moieties than in the occupied molecular orbitals. This demonstrates that, without the ethynyl moiety spacers, the ligand-centered transitions are significantly altered and the pyridyl π-systems contribution to the observed optical properties is greatly increased.

Also, like **10**-PH_3, **11**-PH_3, and **12**-PH_3, it was determined that rhomboid **13**-PH_3 has a large charge transfer between molecular orbitals 328 (HOMO) and 329 (LUMO). Molecular orbital 328 has 98.79% of the electron density on the organo-Pt(II) acceptor unit and 0.31% on the ligand, while in molecular orbital 329 there is 3.35% on the organo-Pt(II) acceptor unit and 95.48% on the ligand.

CONCLUSION

A series of novel Pt(II)-metallacycles were synthesized, and their photophysical properties were investigated experimentally and computationally. During this investigation it was determined that the emissive properties of bis(phosphine) Pt(II) metallacycles arise from ligand-centered transitions involving π-type symmetry molecular orbitals that extend onto the metal center. Interestingly, an endohedral aniline rhomboid **11** had markedly different photophysical properties than those of the ligand **6** used for its construction. Rhomboid **11** has a low-energy excited state that are in the visible regime, and the assembly emits at wavelengths above 500 nm. This novel property makes **11** a promising candidate for applications such as bioimaging and biosensing, since the degradation of the rhomboid can be monitored by its fluorescence.

Currently, there are ongoing efforts to probe the metal center and its effect on the photophysical properties of the endohedral aniline rhomboid **11**. By altering the electronic nature of the ancillary phosphine ligands, it is our intention to synthesize red-shifted rhomboids that retain the novel properties demonstrated in this work.

EXPERIMENTAL PROCEDURES

General Information. 3,5-Diiodoaniline[124] (**1**), *m*-bis(pyridin-4-ylethynyl)benzene[109] (**2**), and 2,9-bis[*trans*-Pt(PEt_3)$_2$$NO_3$]-phenanthrene[125] (**9**) were prepared using known procedures. 2,6-Dibromoaniline was purchased from Sigma-Aldrich. Deuterated solvents were purchased from Cambridge Isotope Laboratory (Andover, MA). ^{1}H, ^{31}P{^{1}H}, and ^{13}C NMR spectra were recorded on a Varian 300 spectrometer, and the mass spectra were recorded on a Micromass LCT Premier XE ToF mass spectrometer using electrospray ionization with a MassLynx operating system. The ESI-MS samples were dissolved in methylene chloride and then diluted with acetone unless otherwise noted. All ^{31}P{^{1}H} spectra were referenced using a 10% H_3PO_4(aq) solution. Elemental Analysis was performed by Atlantic Microlab, Inc.

Ligand Synthesis. *3,5-Diethynylaniline (**3**).* A Schlenk flask was charged with 1.035 g (3.001 mmol) of 3,5-diiodo-aniline, 693.5 mg (20.00 mol %) of Pd(PPh_3)$_4$, and 114.3 mg (20.00 mol %) of CuI. The Schlenk flask was evacuated and placed under positive N_2 pressure. Next, 30 mL of distilled THF, 10 mL of dry Et_3N, and 5.0 mL (35 mmol) of trimethylsilylacetylene were added via syringe. The reaction mixture was stirred for 4 h at room temperature before placing the Schlenk flask in a 60 °C oil bath for 20 h. The solvent was removed by reduced pressure. The crude product, yellow oil, was isolated after column chromatography (mobile phase, 5:1 hexanes/EtOAc). The crude product was then placed into a round-bottom flask, and 25 mL of a MeOH/KOH (1 g) solution was added. The mixture was allowed to stir for 24 h. After removal of the solvent by reduced pressure, the product was isolated by column chromatography (mobile phase, 2:1 hexanes/EtOAc): 280 mg (65% yield); ^{1}H ($CDCl_3$, 300 MHz) δ 7.02 (t, 1H, Ar*H*, J = 1.32 Hz), δ 6.78 (d, 2H, Ar*H*, J = 1.32 Hz), δ 3.75 (s, 2H, NH_2), δ 3.01 (s, 2H, C*H*); ^{13}C ($CDCl_3$, 75 MHz) δ 146.38 (1C), δ 126.34 (1C), δ 123.32 (2C), δ 119.06 (2C), δ 83.08 (2C), δ 77.39 (2C); ESI-MS $[M+H]^+$ 142.07. Anal. Calcd for $C_{10}H_7N$: C, 85.08; H, 5.00; N, 9.92. Found: C, 84.07; H, 9.43; N, 4.93.

*2,6-Diethynylaniline (**4**).* A Schlenk flask was charged with 3.0 g (0.012 mol) of 2,6-dibromoaniline, 10 mol % of CuI (0.23 g), and 10 mol % Pd(PPh_3)$_4$ (1.4 g). The Schlenk flask was then evacuated via reduced pressure and backfilled with N_2. Next, 20 mL of distilled THF and 20 mL of dry Et_3N were added via syringe. Last, 10 equiv of acetylene-TMS (17 mL) was added. The reaction was heated to 60 °C and allowed to stir for 48 h. After cooling, the solvent was removed, and the compound was purified by column chromatography (mobile phase, 10% EtOAc/hexanes). The resulting crude mixture, yellow oil, was used during the next step. A round-bottom flask was charged with the crude mixture from the previous step. A KOH/MeOH solution

Table 4. Wavelength, Molecular Orbitals Involved, Oscillator Strength, and Description for Each Electronic Transition Predicted for 13-PH_3

wavelength/nm	orbital transitions		oscillator strength, f	description
378.2	323 → 330	HOMO−5 → LUMO+1	0.5194	loss of e^- density from aniline nitrogen
	324 → 329	HOMO−4 → LUMO		

dx.doi.org/10.1021/ja3036515 | J. Am. Chem. Soc. 2012, 134, 10607−10620

was prepared by dissolving 1 g into 25 mL. The KOH/MeOH solution was then added to the round-bottom flask, and the mixture was allowed to stir overnight. The solvent was then removed by reduced pressure, and the compound was purified by column chromatography (mobile phase, 30% EtOAc/hexanes): 0.98 g (58% yield) of a yellow solid was afforded; ^{1}H ($CDCl_3$, 300 MHz) δ 7.30 (d, 2H, *Ar*H, J = 7.68 Hz), δ 6.61 (t, 1H, *Ar*H, J = 7.71 Hz), δ 4.86 (bs, 2H, N*H*$_2$), δ 3.41 (s, 2H, C*H*); ^{13}C ($CDCl_3$, 75 MHz) δ 133.59 (1C), δ 117.14 (2C), δ 106.40 (1C), δ 98.81 (2C), δ 83.16 (2C), δ 80.20(2C); ESI-MS $[M+H]^+$ 142.07. Anal. Calcd for $C_{10}H_7N$: C, 85.08; H, 5.00; N, 9.92. Found: C, 83.32; H, 5.15; N, 9.63.

*3,5-Bis(4-pyridylethynyl)aniline (**5**).* A Schlenk flask was charged with 275 mg (1.95 mmol) of 3,5-diethynylaniline, 225 mg (10.0 mol %) of $Pd(PPh_3)_4$, 37.1 mg (10.0 mol %) of CuI, and 758 mg (3.89 mmol) of 4-bromopyridine hydrochloride. The Schlenk flask was evacuated and charged with N_2. Next, 20 mL of distilled THF and 20 mL of dry Et_3N were added via syringe. The reaction mixture was stirred at 60 °C for 48 h. The solvent was removed by reduced pressure, and the product was purified via column chromatography (mobile phase, 10:1 EtOAc/hexanes): 82% yield; ^{1}H ($CDCl_3$, 300 MHz) δ 8.61 (d, 4H, H$_\alpha$-Py, J = 5.88 Hz), δ 7.36 (d, 4H, H$_\beta$-Py, J = 5.91 Hz), δ 7.13 (bs, 1H, Ar*H*), δ 6.87 (d, 2H, Ar*H*, J = 0.96 Hz), δ 3.82 (bs, 2H, N*H*$_2$); ^{13}C ($CDCl_3$, 75 MHz) δ 150.06 (4C), δ 146.77 (1C), δ 131.37 (2C), δ 125.76 (5C), δ 123.53 (2C), δ 118.86 (2C), δ 93.4 (2C), δ 86.9 (2C); ESI-MS $[M+H]^+$ 296.03. Anal. Calcd for $C_{20}H_{13}N_3$: C, 81.34; H, 4.44; N, 14.23. Found: C, 80.25; H, 4.50; N, 13.62.

*2,6-Bis(4-pyridylethynyl)aniline (**6**).* First, 0.975 g (6.91 mmol) of 2,6-bis(4-pyridylethynyl)aniline was weighed into a Schlenk flask with 132 mg (10.0 mol %) of CuI, 798 mg (10.0 mol %) of $Pd(PPh_3)_4$, and 2.50 mol equiv (1.34 g) of 4-bromopyridine HCl. The Schlenk flask was then evacuated by reduced pressure and backfilled with N_2. Next, 20 mL of freshly distilled THF and 20 mL of dry Et_3N were added. The mixture was heated to 60 °C and left to stir for 48 h. The solvent was removed by reduced pressure and purified via column chromatography (mobile phase, EtOAc): 450 mg of a bright yellow solid (23% yield); ^{1}H ($CDCl_3$, 300 MHz) δ 8.62 (d, 4H, H$_\alpha$-Py, J = 3.39 Hz), δ 7.41 (d, 2H, H$_\beta$-Py, J = 4.62 Hz), δ 7.38 (d, 4H, Ar*H*, J = 3.48 Hz), δ 6.74 (t, 1H, Ar*H*, J = 4.59 Hz), δ 4.93 (bs, 2H, N*H*$_2$); ^{13}C ($CDCl_3$, 75 MHz) δ 150.13 (4C), δ 149.57 (1C), δ 133.98 (2C), δ 131.26 (1C), δ 125.54 (4C), δ 117.82 (2C), δ 106.74 (2C), δ 94.99 (2C), δ 92.82 (2C), δ 89.99 (2C); ESI-MS $[M+H]^+$ 296.06. Anal. Calcd for $C_{20}H_{13}N_3$: C, 81.34; H, 14.23; N, 4.44. Found: C, 80.56; H, 13.42; N, 4.67.

*2,6-(4-Pyridine)aniline (**8**).* A Schlenk flask was charged with 1.0 g (4.0 mmol) of 2,6-dibromoaniline and 10 mL of degassed DMF (purged with N_2 for 15 min) and kept under N_2 atomosphere. A 2 M solution of Na_2CO_3 was prepared, purged with N_2 for 15 min, and added to the Schlenk flask via syringe. Then, a solution containing 2.5 mol equiv (1.2 g) of pyridine-4-boronic acid and 15 mol % $PdCl_2(PPh_3)_2$ (280 mg) was prepared using 5 mL of degassed DMF and added to the Schlenk flask via syringe. The mixture was heated to 100 °C and allowed to stir for 72 h. The solvent was removed by reduced pressure, and the product was purified via column chromatography (mobile phase, 10% EtOAc/hexanes): 575 mg of a light orange solid (58.0% yield); ^{1}H ($CDCl_3$, 300 MHz) δ 8.67 (d, 4H, H$_\alpha$-Py, J = 5.7 Hz), δ 7.42 (d, 4H, H$_\beta$-Py, J = 6.03 Hz), δ 7.14 (d, 2H, Ar*H*, J = 7.62 Hz), δ 6.92 (t, 1H, Ar*H*, J = 7.95 Hz), δ 3.90 (bs, 2H, N*H*$_2$); ^{13}C ($CDCl_3$, 75 MHz) δ 150.69 (4C), δ 147.51 (2C), δ 140.49 (1C), δ 130.74 (2C), δ 125.52 (2C), δ 124.29 (4C), δ 119.00 (1C); ESI-MS $[M+H]^+$ 248.06. Anal. Calcd for $C_{16}H_{13}N_3$: C, 77.71; H, 16.99; N, 5.30. Found: C, 76.94; H, 16.79; N, 5.28.

*General Procedure for Rhomboid Formation (**10**–**13**).* In a 1:1 stoichiometric fashion, ligand **5**, **6**, **7**, or **8** was added to the 60° bis(phosphine) organoplatinum(II) acceptor **9** in a 2 dram vial. The solids were dissolved in dichloromethane (methanol for **13**) and allowed to stir at room temperature overnight. For rhomboid **13**, the solution was allowed to stir at 55 °C for 24 h. To the resulting homogeneous solution, diethyl ether was added to precipitate the product, which was then isolated and dried under reduced pressure for 4 h and re-dissolved in CD_2Cl_2 for characterization.

***10**:* ^{1}H NMR (CD_2Cl_2, 300 MHz) δ 9.33 (d, 4H, H$_\alpha$-Py, J = 5.58 Hz), δ 8.86 (s, 4H, Phen*H*), δ 8.66 (d, 4H, H$_{\alpha''}$-Py, J = 5.73 Hz), δ 7.91 (d, 4H, H$_\beta$-Py, J = 5.43 Hz), δ 7.78 (d, 4H, H$_{\beta''}$-Py, J = 4.23 Hz), δ 7.59 (d, 12H, Phen*H*, J = 5.61 Hz), δ 7.34 (s, 2H, Ar*H*), δ 7.13 (s, 4H, Ar*H*), δ 4.56 (bs, 4H, -N*H*$_2$), δ 1.3−1.4 (m, 24H, PC*H*$_2$CH$_3$), δ 1.12−1.27 (m, 36H, PCH$_2$C*H*$_3$); ^{31}P {^{1}H} NMR (CD_2Cl_2, 121.4 MHz) δ 8.04 (bs, ^{195}Pt satellites, $^1J_{Pt-P}$ = 2707 Hz); ESI-MS ($C_{116}H_{162}N_{10}O_{12}P_8Pt_4$) m/z [**10**-2ONO$_2$]$^{2+}$ 1396.40; [**10**-3ONO$_2$]$^{3+}$ 909.96. Anal. Calcd for complex ($C_{116}H_{162}N_{10}O_{12}P_8Pt_4$): C, 47.77; H, 5.60; N, 4.80. Found: C, 47.56; H, 5.70; N, 4.77.

***11**:* ^{1}H (CD_2Cl_2, 300 MHz) δ 8.87 (d, 4H, H$_{\alpha'}$-Py, J = 5.79 Hz), δ 8.67 (d, 4H, H$_{\alpha''}$-Py, J = 5.67 Hz), δ 8.59 (s, 4H, Phen*H*), δ 8.25 (d, 4H, H$_{\beta'}$-Py, J = 5.82 Hz), δ 7.74 (d, 4H, H$_{\beta''}$-Py, J = 5.88 Hz), δ 7.78 (s, 2H, H$_b$-Py), δ 7.62 (d, 8H, Phen*H*, J = 4.44 Hz), δ 7.61 (s, 4H, Phen*H*), δ 7.53 (d, 4H, Ar*H*, J = 7.68 Hz), δ 6.72 (t, 2H, Ar*H*, J = 7.68 Hz), δ 6.31 (bs, 4H, -N*H*$_2$), δ 1.3−1.4 (m, 24H, PC*H*$_2$CH$_3$), δ 1.11−1.27 (m, 36H, PCH$_2$C*H*$_3$); ^{31}P{^{1}H} NMR (CD_2Cl_2, 121.4 MHz) δ 12.61 (bs, ^{195}Pt satellites, $^1J_{Pt-P}$ = 2684 Hz); ESI-MS ($C_{116}H_{162}N_{10}O_{12}P_8Pt_4$) m/z [**11**-2ONO$_2$]$^{2+}$ 1396.45; [**11**-3ONO$_2$]$^{3+}$ 909.98. Anal. Calcd for complex + 3DCM ($C_{119}H_{168}Cl_6N_{10}O_{12}P_8Pt_4$): C, 45.07; H, 5.34; N, 4.42. Found: C, 45.36; H, 5.55; N, 4.46.

***12**:* ^{1}H (CD_2Cl_2, 300 MHz) δ 9.36 (d, 4H, H$_{\alpha'}$-Py, J = 5.85 Hz), δ 8.85 (s, 4H, Phen*H*), δ 8.72 (d, 4H, H$_{\alpha''}$-Py, J = 5.76 Hz), δ 8.06 (s, 2H, Ar*H*), δ 7.97 (d, 4H, H$_{\beta'}$-Py, J = 5.82 Hz), δ 7.75−7.82 (m, 10H, H$_{\beta''}$-Py and Ar*H*), δ 7.53−7.63 (m, 12H, Phen*H*), δ 1.28−1.45 (m, 24H, PC*H*$_2$CH$_3$), δ 1.09−1.23 (m, 36H, PCH$_2$C*H*$_3$); ^{31}P{^{1}H} NMR (CD_2Cl_2, 121.4 MHz) δ 13.32 (bs, ^{195}Pt satellites, $^1J_{Pt-P}$ = 2704 Hz); ESI-MS ($C_{116}H_{160}N_8O_{12}P_8Pt_4$) m/z [**12**-2ONO$_2$]$^{2+}$ 1381.44; [**12**-3ONO$_2$]$^{3+}$ 899.97. Anal. Calcd for complex + 2DCM ($C_{118}H_{164}Cl_4N_8O_{12}P_8Pt_4$): C, 46.37; H, 5.41; N, 3.67. Found: C, 46.50; H, 5.78; N, 3.62.

***13**:* ^{1}H (CD_2Cl_2, 300 MHz) δ 9.06 (d, 4H, H$_{\alpha'}$-Py, J = 5.85 Hz), δ 8.77 (s, 4H, Phen*H*), δ 8.69 (d, 4H, H$_{\alpha''}$-Py, J = 5.67 Hz), δ 8.50 (d, 4H, H$_{\beta'}$-Py, J = 4.17 Hz), δ 8.02 (bs, 4H, -N*H*$_2$), δ 7.82 (d, 4H, H$_{\beta''}$-Py, J = 4.14 Hz), δ 7.55−7.65 (m, 12H, Phen*H*), δ 7.44 (d, 4H, Ar*H*, J = 7.65 Hz), δ 7.03 (t, 2H, Ar*H*, J = 7.62 Hz), δ 1.35−1.45 (m, 24H, PC*H*$_2$CH$_3$), δ 1.1−1.27 (m, 36H, PCH$_2$C*H*$_3$); ^{31}P{^{1}H} NMR (CD_2Cl_2, 121.4 MHz) δ 8.97 (bs, ^{195}Pt satellites, $^1J_{Pt-P}$ = 2692 Hz); ESI-MS ($C_{108}H_{162}N_{10}O_{12}P_8Pt_4$) m/z [**13**-2ONO$_2$]$^{2+}$ 1348.41; [**13**-3ONO$_2$]$^{3+}$ 877.27. Anal. Calcd for complex + 2DCM ($C_{110}H_{166}Cl_4N_{10}O_{12}P_8Pt_4$): C, 44.18; H, 5.59; N, 4.68. Found: C, 44.16; H, 5.80; N, 4.67.

*Hexagon **14**.* First, 180° organoplatinum(II) acceptor μ-1,4-phenylenetetrakis(triethylphosphine)bis(1,1,1-trifluoromethanesulfonato-κO)diplatinum (**15**) and ligand **11** were weighed into separate 2 dram vials and dissolved with methylene chloride (0.5 mL for **11** and 1.0 mL for **15**). The clear solution containing **15** was then added dropwise to the yellow solution of **11**. The brightly colored, green solution was then allowed to stir for 24 h at room temperature. The product was precipitated with diethyl ether, isolated, and redissolved in CD_2Cl_2 for characterization: ^{1}H (CD_2Cl_2, 300 MHz) δ 8.61(bs, 24H, H$_\alpha$-Py), δ 7.87 (bs, 24H, H$_\beta$-Py), δ 7.49 (d, 24H, Ar*H*, J = 7.8 Hz), δ 7.05 (bs, 12H, Ar*H*), δ 6.72 (bs, 6H, Ar*H*), δ 5.79 (bs, 12H, N*H*$_2$), δ 1.36 (bs, 144H, PC*H*$_2$CH$_3$), δ 1.00−1.25 (m, 216H, PCH$_2$C*H*$_3$); ^{31}P{^{1}H} NMR (CD_2Cl_2, 121.4 MHz) δ 12.14 (bs, ^{195}Pt satellites, $^1J_{Pt-P}$ = 2716 Hz); ESI-MS ($C_{108}H_{162}N_{10}O_{12}P_8Pt_4$), see Supporting Information for spectra of fragments. Anal. Calcd for complex + 4DCM ($C_{316}H_{470}Cl_8F_{36}N_{18}O_{36}P_{24}Pt_{12}S_{12}$): C, 39.81; H, 4.97; N, 2.64. Found: C, 39.62; H, 4.97; N, 2.69.

UV−Vis and Fluorescence. Absorption spectra were recorded on a Hitachi U-4100 spectrophotometer, and fluorescence spectra were recorded on a Horiba Jobin-Yvon Fluoromax-3 instrument using aerated spectrophotometric-grade dichloromethane (Sigma-Aldrich) at room temperature. The cells used for the following experiments were all 1 cm path length quartz cuvettes from Starna Cells, Inc. Exctinction coefficients were determined by measuring four solutions at concentrations ranging from 0.6 to 30 μM. The molar absorptivities for each solution were then calculated using Beer's law, and the four

dx.doi.org/10.1021/ja3036515 | J. Am. Chem. Soc. 2012, 134, 10607−10620

were averaged. Subsequent samples were then prepared to confirm the extinction coefficients. For fluorescence, metallacycles were freshly prepared for each measurement. The quantum yield for the instrument was determined by cross-calibrating with two standards: quinine sulfate in 0.1 M H_2SO_4 (Φ = 54%) and anthracene in ethanol (Φ = 27%).

DFT and TD-DFT Calculations. All calculations were performed using the Gaussian09 (G09) program package revision B.01,[123] with the Becke three-parameter hybrid exchange and the Lee−Yang−Parr correlation functionals (B3LYP).[119,120] The 6-31G** basis set[121] was used for H, C, N, and P atoms, while the Los Alamos National Laboratories (LANL2DZ)[122] basis set and pseudopotential was used for Pt. All geometry optimizations were performed without a solvent field in C_1 symmetry; the results are in the gas phase. To minimize computational cost, the PEt_3 ligands on Pt were modeled as PH_3 ligands. Orbitals were visualized using Chem3D and GaussView 5.0 with an isovalue of 0.02.

The percentage of platinum, phenanthrene, phosphine, or ligand character in the occupied (canonical) molecular orbitals (MOs) and virtual orbitals discussed for the previous complexes was calculated from a full population analysis,

$$\%\text{orbital character}_{(\text{Pt,phen,phosphine,Lig})} = \frac{\sum \phi^2_{(\text{Pt,phen,phosphine,Lig})}}{\sum \phi^2_{(\text{all})}} \times 100\% \quad (1)$$

where $\sum\varphi_i$ (i = Pt, phen, phosphine, Lig, or all) is the sum of the squares of the eigenvalues associated with the atomic orbital of interest and all of the atomic orbitals in a particular molecular orbital, respectively. The vertical singlet transition energies of the complexes were computed at the TD-DFT level within G09 using the ground-state optimized structure.

■ ASSOCIATED CONTENT

Supporting Information

^{1}H and ^{13}C NMR spectra for compounds **3**, **4**, **5**, **6**, and **8**; ^{1}H and ^{31}P{^{1}H} NMR spectra and ESI-MS spectra for metallacycles **10**−**14**; atom coordinates for the optimized structures of **10**−**13**; the molecular orbitals involved, wavelength, and oscillator strength for each theoretical electronic transition with a non-zero oscillator from the TD-DFT calculation for **10**−**13**. This material is available free of charge via the Internet at http://pubs.acs.org.

■ AUTHOR INFORMATION

Corresponding Author

stang@chem.utah.edu

■ ACKNOWLEDGMENTS

We are grateful to NSF-CHE 0820955 for financial support. We thank Prof. C. D. Poulter for instrumental support and Prof. A. Orendt for insightful discussions on the quantum mechanical calculations.

■ REFERENCES

(1) Ghosh, S.; Chakrabarty, R.; Mukherjee, P. S. *Inorg. Chem.* **2008**, *48*, 549.
(2) Amouri, H.; Desmarets, C.; Moussa, J. *Chem. Rev.* **2012**, *112*, 2015.
(3) Barry, N. P. E.; Therrien, B. *Eur. J. Inorg. Chem.* **2009**, *2009*, 4695.
(4) Chen, Y.-Q.; Wang, X.-Z.; Shao, X.-B.; Hou, J.-L.; Chen, X.-Z.; Jiang, X.-K.; Li, Z.-T. *Tetrahedron* **2004**, *60*, 10253.
(5) Freudenreich, J.; Barry, N. P. E.; Süss-Fink, G.; Therrien, B. *Eur. J. Inorg. Chem.* **2010**, *2010*, 2400.
(6) Fujita, M.; Nagao, S.; Iida, M.; Ogata, K.; Ogura, K. *J. Am. Chem. Soc.* **1993**, *115*, 1574.
(7) Fujita, M.; Yazaki, J.; Ogura, K. *Tetrahedron Lett.* **1991**, *32*, 5589.
(8) Müller, C.; Whiteford, J. A.; Stang, P. J. *J. Am. Chem. Soc.* **1998**, *120*, 9827.
(9) Murase, T.; Otsuka, K.; Fujita, M. *J. Am. Chem. Soc.* **2010**, *132*, 7864.
(10) Sato, H.; Tashiro, K.; Shinmori, H.; Osuka, A.; Murata, Y.; Komatsu, K.; Aida, T. *J. Am. Chem. Soc.* **2005**, *127*, 13086.
(11) Stang, P. J.; Cao, D. H.; Saito, S.; Arif, A. M. *J. Am. Chem. Soc.* **1995**, *117*, 6273.
(12) Vajpayee, V.; Kim, H.; Mishra, A.; Mukherjee, P. S.; Stang, P. J.; Lee, M. H.; Kim, H. K.; Chi, K.-W. *Dalton Trans.* **2011**, 40.
(13) Whiteford, J. A.; Stang, P. J.; Huang, S. D. *Inorg. Chem.* **1998**, *37*, 5595.
(14) Yamauchi, Y.; Yoshizawa, M.; Akita, M.; Fujita, M. *J. Am. Chem. Soc.* **2009**, *132*, 960.
(15) Hembury, G. A.; Borovkov, V. V.; Inoue, Y. *Chem. Rev.* **2007**, *108*, 1.
(16) Mishra, A.; Vajpayee, V.; Kim, H.; Lee, M. H.; Jung, H.; Wang, M.; Stang, P. J.; Chi, K.-W. *Dalton Trans.* **2012**, 41.
(17) Resendiz, M. J. E.; Noveron, J. C.; Disteldorf, H.; Fischer, S.; Stang, P. J. *Org. Lett.* **2004**, *6*, 651.
(18) Breiner, B.; Clegg, J. K.; Nitschke, J. R. *Chem. Sci.* **2011**, 2.
(19) Dydio, P.; Dzik, W. I.; Lutz, M.; de Bruin, B.; Reek, J. N. H. *Angew. Chem., Int. Ed.* **2011**, *50*, 396.
(20) Fiedler, D.; Leung, D. H.; Bergman, R. G.; Raymond, K. N. *Acc. Chem. Res.* **2004**, *38*, 349.
(21) Koblenz, T. S.; Wassenaar, J.; Reek, J. N. H. *Chem. Soc. Rev.* **2008**, 37.
(22) Lee, S. J.; Hupp, J. T. *Coord. Chem. Rev.* **2006**, *250*, 1710.
(23) Lee, S. J.; Lin, W. *Acc. Chem. Res.* **2008**, *41*, 521.
(24) Pluth, M. D.; Bergman, R. G.; Raymond, K. N. *Acc. Chem. Res.* **2009**, *42*, 1650.
(25) Yoshizawa, M.; Klosterman, J. K.; Fujita, M. *Angew. Chem., Int. Ed.* **2009**, *48*, 3418.
(26) Flamigni, L.; Ventura, B.; Oliva, A. I.; Ballester, P. *Chem.—Eur. J.* **2008**, *14*, 4214.
(27) Indelli, M. T.; Chiorboli, C.; Scandola, F.; Iengo, E.; Osswald, P.; Würthner, F. *J. Phys. Chem. B* **2010**, *114*, 14495.
(28) Jensen, R. A.; Kelley, R. F.; Joong Lee, S.; Wasielewski, M. R.; Hupp, J. T.; Tiede, D. M. *Chem. Commun.* **2008**, 1886.
(29) Kelley, R. F.; Lee, S. J.; Wilson, T. M.; Nakamura, Y.; Tiede, D. M.; Osuka, A.; Hupp, J. T.; Wasielewski, M. R. *J. Am. Chem. Soc.* **2008**, *130*, 4277.
(30) Oliva, A. I.; Ventura, B.; Wurthner, F.; Camara-Campos, A.; Hunter, C. A.; Ballester, P.; Flamigni, L. *Dalton Trans.* **2009**, 4023.
(31) Sprafke, J. K.; Kondratuk, D. V.; Wykes, M.; Thompson, A. L.; Hoffmann, M.; Drevinskas, R.; Chen, W.-H.; Yong, C. K.; Kärnbratt, J.; Bullock, J. E.; Malfois, M.; Wasielewski, M. R.; Albinsson, B.; Herz, L. M.; Zigmantas, D.; Beljonne, D.; Anderson, H. L. *J. Am. Chem. Soc.* **2011**, *133*, 17262.
(32) Cotton, F. A.; Lin, C.; Murillo, C. A. *Acc. Chem. Res.* **2001**, *34*, 759.
(33) Cotton, F. A.; Lin, C.; Murillo, C. A. *Proc. Natl. Acad. Sci. U.S.A.* **2002**, *99*, 4810.
(34) Fujita, M. *Chem. Soc. Rev.* **1998**, *27*, 417.
(35) Fujita, M.; Tominaga, M.; Hori, A.; Therrien, B. *Acc. Chem. Res.* **2005**, *38*, 369.
(36) Farha, O. K.; Hupp, J. T. *Acc. Chem. Res.* **2010**, *43*, 1166.
(37) Lee, J.; Farha, O. K.; Roberts, J.; Scheidt, K. A.; Nguyen, S. T.; Hupp, J. T. *Chem. Soc. Rev.* **2009**, *38*, 1450.
(38) Gianneschi, N. C.; Masar, M. S.; Mirkin, C. A. *Acc. Chem. Res.* **2005**, *38*, 825.
(39) Oliveri, C. G.; Ulmann, P. A.; Wiester, M. J.; Mirkin, C. A. *Acc. Chem. Res.* **2008**, *41*, 1618.
(40) Caulder, D. L.; Brückner, C.; Powers, R. E.; König, S.; Parac, T. N.; Leary, J. A.; Raymond, K. N. *J. Am. Chem. Soc.* **2001**, *123*, 8923.
(41) Caulder, D. L.; Raymond, K. N. *Acc. Chem. Res.* **1999**, *32*, 975.
(42) Chakrabarty, R.; Mukherjee, P. S.; Stang, P. J. *Chem. Rev.* **2011**, *111*, 6810.

(43) De, S.; Mahata, K.; Schmittel, M. *Chem. Soc. Rev.* **2010**, *39*, 1555.
(44) Nitschke, J. R. *Acc. Chem. Res.* **2006**, *40*, 103.
(45) Safont-Sempere, M. M.; Fernández, G.; Würthner, F. *Chem. Rev.* **2011**, *111*, 5784.
(46) Northrop, B. H.; Zheng, Y.-R.; Chi, K.-W.; Stang, P. J. *Acc. Chem. Res.* **2009**, *42*, 1554.
(47) Stang, P. J.; Olenyuk, B. *Acc. Chem. Res.* **1997**, *30*, 502.
(48) Seidel, S. R.; Stang, P. J. *Acc. Chem. Res.* **2002**, *35*, 972.
(49) Bar, A. K.; Mostafa, G.; Mukherjee, P. S. *Inorg. Chem.* **2010**, *49*, 7647.
(50) Mahata, K.; Schmittel, M. *J. Am. Chem. Soc.* **2009**, *131*, 16544.
(51) Solladié, N.; Chambron, J.-C.; Sauvage, J.-P. *J. Am. Chem. Soc.* **1999**, *121*, 3684.
(52) Wang, M.; Zheng, Y.-R.; Cook, T. R.; Stang, P. J. *Inorg. Chem.* **2011**, *50*, 6107.
(53) Wang, M.; Zheng, Y.-R.; Ghosh, K.; Stang, P. J. *J. Am. Chem. Soc.* **2010**, *132*, 6282.
(54) Yamanaka, M.; Yamada, Y.; Sei, Y.; Yamaguchi, K.; Kobayashi, K. *J. Am. Chem. Soc.* **2006**, *128*, 1531.
(55) Yamauchi, Y.; Fujita, M. *Chem. Commun.* **2010**, 46.
(56) Zhao, Z.; Zheng, Y.-R.; Wang, M.; Pollock, J. B.; Stang, P. J. *Inorg. Chem.* **2010**, *49*, 8653.
(57) Zheng, Y.-R.; Zhao, Z.; Wang, M.; Ghosh, K.; Pollock, J. B.; Cook, T. R.; Stang, P. J. *J. Am. Chem. Soc.* **2010**, *132*, 16873.
(58) Wang, M.; Lan, W.-J.; Zheng, Y.-R.; Cook, T. R.; White, H. S.; Stang, P. J. *J. Am. Chem. Soc.* **2011**, *133*, 10752.
(59) Zhao, D.; Tan, S.; Yuan, D.; Lu, W.; Rezenom, Y. H.; Jiang, H.; Wang, L.-Q.; Zhou, H.-C. *Adv. Mater.* **2011**, *23*, 90.
(60) Fyles, T. M.; Tong, C. C. *New J. Chem.* **2007**, 31.
(61) Hannon, M. J. *Chem. Soc. Rev.* **2007**, 36.
(62) Hannon, M. J.; Moreno, V.; Prieto, M. J.; Moldrheim, E.; Sletten, E.; Meistermann, I.; Isaac, C. J.; Sanders, K. J.; Rodger, A. *Angew. Chem., Int. Ed.* **2001**, *40*, 879.
(63) Kieltyka, R.; Englebienne, P.; Fakhoury, J.; Autexier, C.; Moitessier, N.; Sleiman, H. F. *J. Am. Chem. Soc.* **2008**, *130*, 10040.
(64) Ma, D.-L.; Che, C.-M.; Yan, S.-C. *J. Am. Chem. Soc.* **2009**, *131*, 1835.
(65) Tashiro, S.; Tominaga, M.; Yamaguchi, Y.; Kato, K.; Fujita, M. *Angew. Chem., Int. Ed.* **2006**, *45*, 241.
(66) Barry, N. P. E.; Edafe, F.; Dyson, P. J.; Therrien, B. *Dalton Trans.* **2010**, 39.
(67) Horcajada, P.; Gref, R.; Baati, T.; Allan, P. K.; Maurin, G.; Couvreur, P.; Férey, G.; Morris, R. E.; Serre, C. *Chem. Rev.* **2012**, *112*, 1232.
(68) Mounir, M.; Lorenzo, J.; Ferrer, M.; Prieto, M. J.; Rossell, O.; Avilès, F. X.; Moreno, V. *J. Inorg. Biochem.* **2007**, *101*, 660.
(69) Ang, W. H.; Grote, Z.; Scopelliti, R.; Juillerat-Jeanneret, L.; Severin, K.; Dyson, P. J. *J. Organomet. Chem.* **2009**, *694*, 968.
(70) Barry, N. P. E.; Edafe, F.; Therrien, B. *Dalton Trans.* **2011**, 40.
(71) Barry, N. P. E.; Zava, O.; Furrer, J.; Dyson, P. J.; Therrien, B. *Dalton Trans.* **2010**, 39.
(72) Linares, F. T.; Galindo, M. A.; Galli, S.; Romero, M. A.; Navarro, J. A. R.; Barea, E. *Inorg. Chem.* **2009**, *48*, 7413.
(73) Therrien, B.; Süss-Fink, G.; Govindaswamy, P.; Renfrew, A. K.; Dyson, P. J. *Angew. Chem., Int. Ed.* **2008**, *47*, 3773.
(74) Vajpayee, V.; Song, Y. H.; Jung, Y. J.; Kang, S. C.; Kim, H.; Kim, I. S.; Wang, M.; Cook, T. R.; Stang, P. J.; Chi, K.-W. *Dalton Trans.* **2012**, *41*, 3046.
(75) Vajpayee, V.; Song, Y. H.; Yang, Y. J.; Kang, S. C.; Kim, H.; Kim, I. S.; Wang, M.; Stang, P. J.; Chi, K.-W. *Organometallics* **2011**, *30*, 3242.
(76) Vajpayee, V.; Yang, Y. J.; Kang, S. C.; Kim, H.; Kim, I. S.; Wang, M.; Stang, P. J.; Chi, K.-W. *Chem. Commun.* **2011**, 47.
(77) Yi, J. W.; Barry, N. P. E.; Furrer, M. A.; Zava, O.; Dyson, P. J.; Therrien, B.; Kim, B. H. *Bioconjugate Chem.* **2012**, *23*, 461.
(78) Zava, O.; Mattsson, J.; Therrien, B.; Dyson, P. J. *Chem.—Eur. J.* **2010**, *16*, 1428.
(79) Schmitt, F.; Freudenreich, J.; Barry, N. P. E.; Juillerat-Jeanneret, L.; Süss-Fink, G.; Therrien, B. *J. Am. Chem. Soc.* **2012**, *134*, 754.
(80) Paul, L. E. H.; Therrien, B.; Furrer, J. *Inorg. Chem.* **2011**, *51*, 1057.
(81) Hui, C.-K.; Chu, B. W.-K.; Zhu, N.; Yam, V. W.-W. *Inorg. Chem.* **2002**, *41*, 6178.
(82) Wong, H.-L.; Tao, C.-H.; Zhu, N.; Yam, V. W.-W. *Inorg. Chem.* **2010**, *50*, 471.
(83) Wong, K. M.-C.; Yam, V. W.-W. *Acc. Chem. Res.* **2011**, *44*, 424.
(84) Adamson, A. W.; Waltz, W. L.; Zinato, E.; Watts, D. W.; Fleischauer, P. D.; Lindholm, R. D. *Chem. Rev.* **1968**, *68*, 541.
(85) Brooks, J.; Babayan, Y.; Lamansky, S.; Djurovich, P. I.; Tsyba, I.; Bau, R.; Thompson, M. E. *Inorg. Chem.* **2002**, *41*, 3055.
(86) Caspar, J. V. *J. Am. Chem. Soc.* **1985**, *107*, 6718.
(87) Chan, S.-C.; Chan, M. C. W.; Wang, Y.; Che, C.-M.; Cheung, K.-K.; Zhu, N. *Chem.—Eur. J.* **2001**, *7*, 4180.
(88) Danilov, E. O.; Rachford, A. A.; Goeb, S. b.; Castellano, F. N. *J. Phys. Chem. A* **2009**, *113*, 5763.
(89) Eryazici, I.; Moorefield, C. N.; Newkome, G. R. *Chem. Rev.* **2008**, *108*, 1834.
(90) Fleischauer, P. D.; Fleischauer, P. *Chem. Rev.* **1970**, *70*, 199.
(91) Forniés, J.; Fuertes, S.; Martín, A.; Sicilia, V.; Lalinde, E.; Moreno, M. T. *Chem.—Eur. J.* **2006**, *12*, 8253.
(92) Goeb, S.; Prusakova, V.; Wang, X.; Vezinat, A.; Salle, M.; Castellano, F. N. *Chem. Commun.* **2011**, 47.
(93) Ho, Y.-M.; Koo, C.-K.; Wong, K.-L.; Kong, H.-K.; Chan, C. T.-L.; Kwok, W.-M.; Chow, C.-F.; Lam, M. H.-W.; Wong, W.-Y. *Dalton Trans.* **2012**, 41.
(94) Kui, S. C. F.; Hung, F.-F.; Lai, S.-L.; Yuen, M.-Y.; Kwok, C.-C.; Low, K.-H.; Chui, S. S.-Y.; Che, C.-M. *Chem.—Eur. J.* **2012**, *18*, 96.
(95) Lees, A. J. *Chem. Rev.* **1987**, *87*, 711.
(96) Pomestchenko, I. E.; Luman, C. R.; Hissler, M.; Ziessel, R.; Castellano, F. N. *Inorg. Chem.* **2003**, *42*, 1394.
(97) Rausch, A. F.; Murphy, L.; Williams, J. A. G.; Yersin, H. *Inorg. Chem.* **2011**, *51*, 312.
(98) Wang, Z.; Turner, E.; Mahoney, V.; Madakuni, S.; Groy, T.; Li, J. *Inorg. Chem.* **2010**, *49*, 11276.
(99) Weinstein, J. A.; Tierney, M. T.; Davies, E. S.; Base, K.; Robeiro, A. A.; Grinstaff, M. W. *Inorg. Chem.* **2006**, *45*, 4544.
(100) Wong, K. M.-C.; Yam, V. W.-W. *Coord. Chem. Rev.* **2007**, *251*, 2477.
(101) Yam, V. W.-W. *Acc. Chem. Res.* **2002**, *35*, 555.
(102) Zhao, G.-J.; Yu, F.; Zhang, M.-X.; Northrop, B. H.; Yang, H.; Han, K.-L.; Stang, P. J. *J. Phys. Chem. A* **2011**, *115*, 6390.
(103) Zhao, G.-J.; Northrop, B. H.; Han, K.-L.; Stang, P. J. *J. Phys. Chem. A* **2010**, *114*, 9007.
(104) Ghosh, S.; Mukherjee, P. S. *Organometallics* **2008**, *27*, 316.
(105) Zhao, G.-J.; Northrop, B. H.; Stang, P. J.; Han, K.-L. *J. Phys. Chem. A* **2010**, *114*, 3418.
(106) Flynn, D. C.; Ramakrishna, G.; Yang, H.-B.; Northrop, B. H.; Stang, P. J.; Goodson, T. *J. Am. Chem. Soc.* **2010**, *132*, 1348.
(107) Kaloudi-Chantzea, A.; Karakostas, N.; Raptopoulou, C. P.; Psycharis, V.; Saridakis, E.; Griebel, J.; Hermann, R.; Pistolis, G. *J. Am. Chem. Soc.* **2010**, *132*, 16327.
(108) Johnson, A. M.; Moshe, O.; Gamboa, A. S.; Langloss, B. W.; Limtiaco, J. F. K.; Larive, C. K.; Hooley, R. J. *Inorg. Chem.* **2011**, *50*, 9430.
(109) Amoroso, A. J.; Thompson, A. M. W. C.; Maher, J. P.; McCleverty, J. A.; Ward, M. D. *Inorg. Chem.* **1995**, *34*, 4828.
(110) Ghosh, K.; Hu, J.; Yang, H.-B.; Northrop, B. H.; White, H. S.; Stang, P. J. *J. Org. Chem.* **2009**, *74*, 4828.
(111) Zheng, Y.-R.; Northrop, B. H.; Yang, H.-B.; Zhao, L.; Stang, P. J. *J. Org. Chem.* **2009**, *74*, 3554.
(112) Zheng, Y.-R.; Stang, P. J. *J. Am. Chem. Soc.* **2009**, *131*, 3487.
(113) Knee, J. L.; Johnson, P. M. *J. Chem. Phys.* **1984**, *80*, 13.
(114) Rückert, I.; Demeter, A.; Morawski, O.; Kühnle, W.; Tauer, E.; Zachariasse, K. A. *J. Phys. Chem. A* **1999**, *103*, 1958.
(115) Scheps, R.; Florida, D.; Rice, S. A. *J. Chem. Phys.* **1974**, *61*, 1730.

(116) Yang, J.-S. *PATAI'S Chemical Functional Groups*; John Wiley & Sons, Ltd.: New York, 2009.
(117) Lewis, F. D.; Hougland, J. L.; Markarian, S. A. *J. Phys. Chem. A* **2000**, *104*, 3261.
(118) *Substituent Constants for Correlation Analysis in Chemistry and Biology*; Hansch, C. L. A., Ed.; Wiley-Interscience: New York, 1979.
(119) Becke, A. D. *J. Chem. Phys.* **1993**, *98*, 5648.
(120) Lee, C.; Yang, W.; Parr, R. G. *Phys. Rev. B* **1988**, *37*, 785.
(121) Hehre, W. J.; Ditchfield, R.; Pople, J. A. *J. Chem. Phys.* **1972**, *56*, 2257.
(122) Hay, P. J.; Wadt, W. R. *J. Chem. Phys.* **1985**, *82*, 299.
(123) Frisch, M. J.; G. W. T., Schlegel, H. B.; Scuseria, G. E.; ,; Robb, M. A.; J. R. C., Scalmani, G.; Barone, V.; Mennucci, B.; ,; Petersson, G. A.; H. N., Caricato, M.; Li, X.; Hratchian, H. P.; ,; Izmaylov, A. F.; J. B., Zheng, G.; Sonnenberg, J. L.; Hada, M.; ,; Ehara, M.; K. T., Fukuda, R.; Hasegawa, J.; Ishida, M.; Nakajima, T.; ,; Honda, Y.; O. K., Nakai, H.; Vreven, T.; Montgomery, J. A.; , Jr.,; J. E. Peralta, F. O., Bearpark, M.; Heyd, J. J.; Brothers, E.; ,; K. N. Kudin, V. N. S., Keith, T.; Kobayashi, R.; Normand, J.; ,; Raghavachari, K.; A. R., Burant, J. C.; Iyengar, S. S.; Tomasi, J.; ,; Cossi, M.; N. R., Millam, J. M.; Klene, M.; Knox, J. E.; Cross, J. B.; ,; Bakken, V.; C.A., Jaramillo, J.; Gomperts, R.; Stratmann, R. E.; ,; Yazyev, O.; A. J. A., Cammi, R.; Pomelli, C.; Ochterski, J. W.; ,; R. L. Martin, K. M., Zakrzewski, V. G.; Voth, G. A.; ,; Salvador, P.; J. J. D., Dapprich, S.; Daniels, A. D.; Farkas, O.; J. B. F., Ortiz, J. V.; Cioslowski, J.; ,; Fox, D. J. *Gaussian*; Gaussian, Inc.: Wallingford, CT, 2010.
(124) Chimenti, F.; Bolasco, A.; Secci, D.; Chimenti, P.; Granese, A. *Synth. Commun.* **2004**, *34*, 2549.
(125) Kryschenko, Y. K.; Seidel, S. R.; Arif, A. M.; Stang, P. J. *J. Am. Chem. Soc.* **2003**, *125*, 5193.